Title
Enhanced AHS Safety Through the Integration of Vehicle Control and Communication

Authors
Hedrick, J. K.
Sengupta, R.
Xu, Q.
et al.

Publication Date
2003-09-01

CALIFORNIA PATH PROGRAM
INSTITUTE OF TRANSPORTATION STUDIES
UNIVERSITY OF CALIFORNIA, BERKELEY

Enhanced AHS Safety Through the Integration of Vehicle Control and Communication

J.K. Hedrick, R. Sengupta, Q. Xu, Y. Kang, C. Lee
University of California, Berkeley

California PATH Research Report
UCB-ITS-PRR-2003-27

This work was performed as part of the California PATH Program of the University of California, in cooperation with the State of California Business, Transportation, and Housing Agency, Department of Transportation; and the United States Department of Transportation, Federal Highway Administration.

Report for Task Order 4210

September 2003

ISSN 1055-1425

Enhanced AHS Safety Through the Integration of Vehicle Control and Communication

Final Report

PATH Task Order 4210

J. K. Hedrick
R. Sengupta
Q. Xu
Y. Kang
C. Lee

Mechanical Engineering Department
University of California at Berkeley
Berkeley, CA 94720

Abstract

We comparatively assess the influence of adaptive cruise control (ACC) and cooperative adaptive cruise control (CACC) systems on highway traffic behaviors. The primary goal is to study the design and implementation of vehicle-vehicle/roadside-vehicle communication, which enhances an ACC system to a CACC one. In addition, the impact of market penetration of ACC/CACC vehicles and controller aggression are also evaluated. Two simulation works are presented. The microscopic work simulates a single ACC/CACC vehicle using MATLAB/SIMULINK. A cut-in scenario and a braking scenario are tested. Vehicle-vehicle communication saves control effort in the former scenario, while shows little effect in the latter. In the macroscopic work we simulate ACC/CACC controlled highway merging with SHIFT language. The results show beneficial effects of communication in terms of braking effort, average velocity, waiting-to-merge queue length, and main lane traffic shock wave caused by merging. The higher the market penetration of controlled vehicles the better the system performs. The aggressiveness of controller has mixed influence, which provides a tradeoff between efficiency and safety.

We study the wireless communication among highway vehicles. A vehicle-vehicle Location-Based Broadcast (LBB) communication protocol is designed to meet highway safety applications' communication requirements. The analytical expressions of the performance of the protocol in terms of probability of transmission failure and channel occupancy are derived with commonly satisfied assumptions. The optimal relation between the performance and design parameters is obtained from the expressions. The sensitivity of the protocol performance is tested for various communication conditions as well as highway traffic conditions. Feasible combinations of the communication and highway traffic parameters are found for certain requirements on protocol performance. The analysis is conducted in accordance to the communication condition in the newly-assigned 5.9 GHz Dedicated Short Range Communication (DSRC) spectrum.

More experiments are done to find out the factors that influence the slip measurements in order to refine our results of friction coefficient estimation. To obtain the circumferential velocity of the wheel, the exact tire radius is needed. The change in the spring constant based on tire air pressure is obtained, and also the increase in tire radius due to the faster velocity is considered. The normal force applied on each wheel due to the vehicle pitch

motion resulting from acceleration and deceleration is also estimated using static vehicle model. Brake torque sensor and accelerometer are used to find the normal force. Using the estimated normal force and road force, the tire-road friction coefficient is obtained. The characteristics of the friction coefficient and slip curve are studied on different road conditions with the refined slip measurements.

An originally proposed slip-based controller does not seem to work very well in an practical situation due to actuator time delay. However, experimental results show that the existing nonlinear controller with the limited slip assumption shows good performance even in an emergency braking situation. Therefore, instead of using different control algorithm, this research focuses on the control strategies dedicated to emergency situation for the platoon.

In order to integrate the benefits from the communication and friction coefficient estimation technique, a safe control strategy is considered in the situation when the platoon of vehicles needs to decelerate rapidly. It is assumed that we have the knowledge of friction coefficients between road and tire and our vehicles are equipped with proper communication methods. Then, the theoretical bounds for the reference trajectory accelerations are calculated that do not cause the actuator saturation using linear vehicle and controller model.

Keywords: Ad-hoc networks, Vehicle-vehicle communication protocol, Cooperative adaptive cruise control, Cooperative estimation, Friction coefficient, String stability, Emergency braking, Platoon.

Contents

List of Figures

Chapter 1

Introduction

This final report presents research findings obtained under PATH Task Order 4210, a three-year project devoted to catalyzing AHS (Automated Highway System) deployment and improving AHS safety through the integration of communication and control. This project is a continuation of PATH MOU 388 and the findings of the PATH MOU 388 will be briefly presented in the introduction. Then, from the next chapter, new researches done in the following Task Order 4210 will be described.

One of the main factors separating true *intelligent highway systems* like the PATH concept from *collections of intelligent cruise control vehicles* is the presence of an inter-vehicle communication network to coordinate vehicle maneuvers. Unfortunately, automotive communication networks have been slow to appear on roadways, largely due to two problems: First, the networking technology to handle highly mobile networks has been slow to develop, and second, few applications have been developed that use these networks.

In the MOU 388, we developed a new communication protocol for vehicle-to-vehicle ad-hoc networks. Simulation results that we present here show that the new proposed MAC protocol can transmit with probability of over 97% the messages which cannot get through in the old protocol.

To help solve the application problem, we developed two new ways for vehicle-to-vehicle networks to improve highway safety and convenience. The first of these applications,"Cooperative Adaptive Cruise Control," uses inter-vehicle communication to improve on adaptive cruise control systems. Simulation results in this report show that during cut-in and hard braking situations, a communicated "virtual brake light" significantly decreases the accelerations that the adaptive cruise control system needs to maintain safety

distances. The second of these applications—a new concept, which we dub "cooperative estimation"—uses inter-vehicle communication to generate estimates of important driving quantities that are more useful than any vehicle on the highway could produce by itself. We apply the cooperative estimation concept to travel time estimation and road condition estimation, and simulation results show that inter-vehicle communication can significantly improve travel time and coefficient of friction estimates.

Estimating road condition is of particular importance for AHS, so in addition to developing the cooperative road condition estimator, we also pursued the road friction estimation problem through experimental investigations at the vehicle level. The fruit of these investigations is a new road condition estimator that works during braking and avoids using dedicated road condition sensors. Results from our own on-vehicle extensive testing, combined with results from a handful of new papers in the literature, indicate that road condition estimators similar to ours have strong potential to deliver enhanced highway safety safety at minimal added cost.

Chapter 2

Communication-aided Cooperative Adaptive Cruise Control

2.1 Introduction

In recent years lots of research efforts are initiated to enhance the safety and efficiency of highway/urban traffic with the aid of wireless communication and automatic control techniques. Both ad hoc wireless network based vehicle-vehicle (V-V) communication and infrastructure-based roadside-vehicle (R-V) communication are considered as the candidate implementation of such system [10] [27] [1] [39] [29] [49] [33]. Aware of the great benefit such communication system could bring, FCC proposed the allocation of 5.9GHz band spectrum specifically to the national ground transportation safety and productivity. The on-going standardization process of this Dedicated Short Range Communication (DSRC) band inspires further research activities in the field [1].

Adaptive Cruise Control (ACC) systems are the first driver control assistance systems entering the market that have the potential to influence traffic flow characteristics [43]. In conventional cruise control the vehicle is commanded to maintain a preset velocity, regardless of the traffic environment. With adaptive cruise control, the vehicle tries to maintain a desired range with the preceding vehicle and to match the preceding velocity on basis of the measurement from forward-looking sensors (typically millimeter-wave

radar or infrared laser). When V-V/R-V communication is conjoined with ACC, the system becomes Cooperative Adaptive Cruise Control (CACC) system. Besides the sensor measurements, CACC vehicles also receive information communicated by the preceding vehicle and other relevant vehicles. All these vehicles cooperatively perform control maneuvers. ACC equipped product vehicles are already in market, while CACC is an active research field attracting high degree of interest.

We incorporate the design of V-V/R-V communication system with that of the ACC/CACC system, and study the impact of such incorporation on the behavior of highway vehicles on both microscopic and macroscopic level. In addition, some other design parameters of the system, namely the market penetration and controller aggressiveness, are also studied to understand their effects. The research reported here is simulation by nature. This choice is due, on one hand, to the difficulty in the analytical solution of such complicated system as highway traffic, and on the other, to the hardship and cost in collecting large fleet of ACC/CACC vehicles to conduct experiment. The simulation results serve as the guideline for future analytical and experimental work.

The rest part of the chapter is organized as follows. Section 2.2 summarizes relevant previous work in publication. Section 2.3 describes the simulation scenario. Section 2.4 is the system modeling and implementation. Section 2.5 reports and discusses the results of simulation.

2.2 Previous Work

The literature is well supplied with papers analyzing the effects introduced by ACC vehicles to the traffic behavior (congestion, delay, safety, emissions, fuel consumption, etc.). All of the papers studying macroscopic behavior have been based on analytical models and/or simulations since there are not yet enough ACC vehicles to perform a direct experimental evaluation. Some microscopic works used experiments [26] and driving simulator [46]. More extensive literature review up to their publication dates can be found in [43] and [50].

Much of the interest concentrates on the impact of the ACC system on the traffic flow capacity [43] [50] [13] [36] [11] [32]. Although it is hoped that the introduction of ACC system could increase the capacity, mixed results are found and the performance is of course dependent on the system design

and the parameter choice. Zwaneveld and van Arem [50] reviewed a variety of prior papers and concluded that the general tendency was to show little potential for congestion reduction (capacity increase), but some potential to improve traffic flow stability. Chang and Lai [11] showed expected traffic flow effects at market penetrations of 30, 50, 80 and 100% ACC, with a nonlinear increase in traffic flow capacity, leading to a maximum of 2750 vehicles/lane/hour with all ACC vehicles. At the same time, some work indicates that the application of ACC increases flow capacity only marginally or even decreases the capacity under some circumstance. Cremer et. al. in [13] did a simultaneous comparison of one macroscopic and four microscopic models for predicting the effects of ACC (at a time gap of 1.2 s) on traffic flow. Their results showed little change in traffic flow at ACC market penetrations of 40% and 70%. The results of [32] showed that the ACC with a time-gap setting of 1.2 s would leave traffic flow capacity essentially unchanged from the baseline manual driving conditions, while the time gaps of 1.0 s and 1.4 s could cause noticeable, but small, increases and decreases in flow capacity respectively at the highest market penetration rates. It was necessary to reduce the time gap to 0.8 s to generate capacity increases in the 10% range at market penetrations of 50% or higher. It seems that the divergence of the highway system modeling, the ACC controller design, and simulation and experiment tools prohibits us to draw easy conclusion on the effect of ACC system on the highway traffic flow capacity.

The performance of ACC system on smoothing and stabilizing highway traffic and reducing shock wave is another focus of interest, and the results in this aspect are more encouraging. Many previous works indicate that ACC vehicles smooth traffic flow by filtering the impact of rapidly accelerating lead vehicles, therefore making the traffic more stable and have less shock waves [43] [8] [42] [47] [14]. Analytical results regarding some particular concepts of stability of ACC system were also obtained, e.g. string stability [8] and traffic flow stability [14]. Other performance variables studied are trip time, trip delay [27] [47], traffic speed and time gaps [42]. ACC system has beneficial effect on them to various degree. Besides the macroscopic behavior the performance of individual vehicle under ACC is also studied [27] [23] [26]. Apparently the ACC system has more definitive benefit on driving comfort and safety than on traffic flow.

The concept of CACC, i.e. communication-aided ACC, is new and relevant literature is rare. Shladover, et. al. [43] compared the performance of human driver, ACC, and CACC system. In their CACC system design,

the preceding vehicle continuously transmits the acceleration and braking capacity information to the follower via point-to-point vehicle-vehicle communication. Using the information together with the radar measurement, the CACC system drives the vehicles with much smaller range than in either ACC or human-driven cases, without sacrificing safety. Therefore the capacity of highway is greatly enhanced. Part of our work is based on the simulation they built, but as we will see that our communication system design in CACC is different from theirs.

Hedrick, et al [23] built a thorough vehicle model for a BMW test vehicle. They experimentally validated all the components in the model, and implemented the model with SIMULINK and C language. An ACC controller was designed using sliding surface technique. Gain scheduling was applied to the resulting controller for different combinations of range and range rate. The controller was integrated in the SIMULINK vehicle model and tested in various scenarios. It was shown that the ACC controller performs well in all the cases considered. Their simulation was on the level of individual vehicle, therefore the macroscopic behavior of the traffic flow could not be observed. Part of our simulation is based on their work.

2.3 Simulation Scenarios

Two simulation studies are presented in this chapter. The first simulates the response of a single CACC vehicle to the changing highway traffic environment, and the second one is the simulation of two highways carrying CACC vehicles that merge. For presentation convenience we name them respectively as One-vehicle CACC simulation (OVC), and Highway Merging Control simulation (HMC).

2.3.1 One-vehicle CACC simulation (OVC)

Two scenarios, Braking and Cut-in, are simulated in OVC.

In Braking scenario, two vehicles are driving in the same lane with the follower being automatically controlled. We compare the behavior of the following vehicle when its control system is CACC with the case when the control system is ACC. In the simulation, the preceding vehicle brakes and the follower applies a proper braking in response to maintain the desired range and match the preceding velocity. In ACC scheme, the follower mea-

sures the range and range rate with radar and sensors. The range rate is differentiated to obtain acceleration, and the braking of the preceding vehicle is detected from the sign of acceleration. With V-V communication, whenever the preceding vehicle brakes, it transmits a "brake light" message to the CACC following vehicle. The CACC vehicle, upon receiving the message, brakes strongly enough for safety but not enough for passenger discomfort. Response time is increased by replacing the sum of sensor delay and computational delay with communication delay. The preceding vehicle is assumed to have V-V communication capability when the follower is a CACC vehicle.

In Cut-in scenario, initially an ACC/CACC vehicle is following its preceding vehicle. Then a third vehicle in the adjacent lane cuts in between the two vehicles, and becomes the new preceding vehicle of the ACC/CACC vehicle. Without communication, the ACC vehicle detects the cut-in vehicle when the latter passes the lane border. The ACC controller then commands the vehicle to brake, sometime abruptly, to make space in front for the cut-in vehicle. With CACC system using V-V communication, the cut-in vehicle transmits the equivalent of a "turning light" message to the CACC vehicle at the instant it starts the cut in maneuver from the centerline of the adjacent lane. The CACC vehicle then has approximately half of lane change time to slow down and make space for the cut-in vehicle. In CACC scheme we assume the cut-in vehicle and the CACC vehicle to have V-V communication capability, while the "old" preceding vehicle does not have to communicate.

2.3.2 Highway Merging CACC Simulation (HMC)

In HMC, vehicles merge into the main lane from a merge-in lane, and the two lanes join at a merge-in point (MP), as illustrated in Figure 2.1. In the figure cars B and C are the main lane vehicles, and car A is in the merge-in lane.

Some or all of the main lane vehicles are ACC/CACC controlled while others are driven by humans. The market penetration of the ACC/CACC vehicles in the main lane is controllable. Therefore we can study the interaction between the human-driven vehicles and the controlled vehicles, as well as the effect of different market penetration of the controlled vehicles. Notice that in this chapter we do not study the interactions between ACC and CACC, but their respective interactions with human drivers. Therefore in any mixed case in our simulation, the vehicles on the highway are composed of either ACC vehicles mixed with human-driven ones or CACC vehicles mixed with

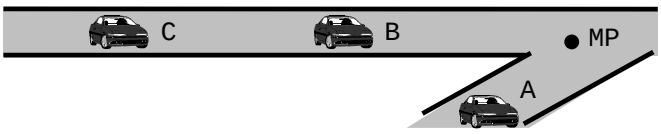

Figure 2.1: Highway Layout of HMC

human-driven ones, i.e., ACC vehicles and CACC vehicles never co-exist in the simulation.

The procedure of merge-in in CACC scheme is as follows.

1. *Head merging vehicle is generated*

   At the instant the first vehicle in the merge-in lane enters the main lane, the second vehicle in the lane becomes the new "head merging vehicle". For presentation convenience, assume car A in Fig 2.1 is the new head merging vehicle. In CACC system, at the instant it becomes the head merging car, car A broadcasts a message to all the main lane vehicles within its communication range. The communication could be realized by either V-V communication with A being the broadcaster, or R-V communication with the aid of a roadside station at MP. The message contains the position of the merge-in point and the time needed by vehicle A to enter the main lane. If A is driving at the instant it becomes the head merging vehicle, this time is needed for A to drive from its position at that instant to merge-in point. If A is stationary at the merge-in point when it becomes the head (e.g. when there is a queue formed in the merging lane), we assume a metering light at the MP commanding A to wait for a certain amount of time before it attempts to merge. The length of the time the head merging vehicle waits is set to be the reciprocal of the input flow rate of the merging lane. For example, for merge-in lane flow rate of 1200 vehicles/hour/lane, the average waiting time is about 3 seconds.

2. *Head merging vehicle drives to or waits at merge-in point*

   After receiving the warning message from the head merging vehicle, each main lane vehicle determines the relevance of the message to itself. If a main lane vehicle C (see Figure 2.1) finds that at the anticipated time when vehicle A arrives in the main lane, A will cut in between C and its current preceding vehicle B, C regards the message as relevant.

In response to the relevant message, C brakes promptly but smoothly to increase the gap between itself and vehicle B. If a car finds a message irrelevant, it simply discards it. The information needed in making the decision includes: the position of merge-in point and the predicted time A will merge in (obtained from the communicated message, which is in turn obtained from GPS and/or digital map), the position of C and its velocity (obtained from e.g. GPS and speedometer), and position and velocity of the preceding vehicle B (obtained from radar measurements).

3. *Head merging vehicle waits for acceptable gap in main lane*

   When it arrives at the MP, the head merging vehicle stops and observes the gap between the passing main lane vehicles. It waits to merge until an acceptable gap appears. If the main lane traffic is too busy such that the head merging vehicle has to wait for excessively long time, a queue of waiting cars forms in the merge-in lane. Notice that the waiting period in this step is different from the one in the step (2). The waiting in last step is either commanded by the metering light or required for the head merging vehicle to drive to the MP, therefore it is unavoidable and is about the same for all merging vehicles. However the waiting in this step is for the head merging vehicle to find a safe gap, and the length of the waiting is random depending on the main lane traffic.

4. *Head merging vehicle merges in*

   The head merging vehicle merges in the gap it feels safe. At this instant, the main lane vehicle right behind it sees the merging vehicle, and responds by necessary braking. The head merging vehicle's initial velocity in the main lane is designed to be that of the main lane vehicle right in front of it. Now the second vehicle in the merging lane, if any, becomes the new head merging vehicle, and we are back in step one and the above procedure is repeated.

In the ACC scheme there is no communication. Therefore we have only the last two steps in the above procedure. We repeat them here for clarity.

1. *Head merging vehicle waits for acceptable gap in main lane*

2. *Head merging vehicle merges in*

Clearly, there is no cooperation between the merging vehicles and the main lane vehicles.

2.4 System Modeling and Design

This section describes the models implemented in the simulation and the controller design. The OVC models are implemented with MATLAB/SIMULINK. The HMC simulation is built using SHIFT, a language developed by California PATH for describing dynamic network of hybrid automata [2]. We give detailed explanation of three critical components, i.e. vehicle model, controller design, and communication system. These three parts essentially cover the whole OVC system, however there are other components in HMC which are independent of the above three models. We describe these HMC components in the final part of this section.

2.4.1 Vehicle Model

Vehicle model in OVC

The OVC uses the vehicle model of a BMW test vehicle [23]. The model includes the following components, each is further composed of sub-models:

- longitudinal vehicle dynamics
- Wheel dynamics
- Unlocked engine dynamics
- Torque converter
- Lockup logic
- Gear shifting, and
- Throttle/brake actuator models

Each part of the model is experimentally validated with the vehicle driven in test track or urban streets. The parameters are either estimated from experiment results or provided by the manufacturer. The well-studied vehicle

model enables us to observe the performance of the controller under the influence of the nonlinear dynamics of the mechanical components of a vehicle. The details of modeling and validation of each component of the vehicle model are summarized in [23].

The OVC models are implemented in simulation using SIMULINK package of Matlab. SIMULINK uses a graphical interface to build models in block diagram form. Figure 2.2 shows the upper layer of the SIMULINK vehicle model. The upper portion of this picture contains the vehicle model subsystems and the lower portion contains the controller subsystems.

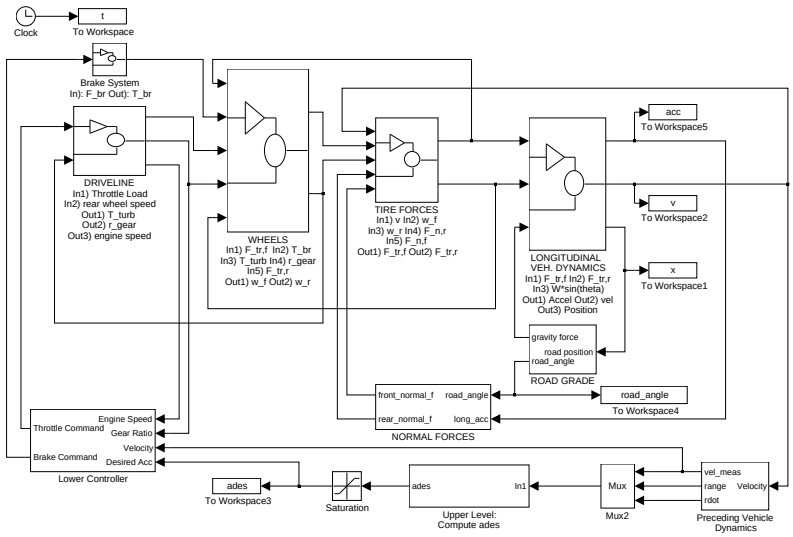

Figure 2.2: SIMULINK diagram of vehicle model and ACC/CACC controller

We now give a brief overview of the system by following the flow of the model from left to right. In the upper left of Figure 2.2 are the brake and driveline subblocks. The two actuators inputs, brake and throttle load, enter these blocks. Specifically, the brake subsystem takes in the brake actuator input load and outputs the net brake torque. This net brake torque enters the wheel dynamics block, which implements the wheel dynamics equations for each wheel. The driveline block implements the engine map, torque converter equations, lockup logic, and gear map. The inputs to this block are throttle load and rear wheel angular velocity and the outputs are engine speed, gear ratio and torque converter output torque. The previously mentioned wheel

dynamics block uses the brake torque (from the brake subsystem) and the turbine torque and gear ratio (both from the driveline block) as inputs. It also inputs the front and rear tractive forces (which are generated by the tire forces block, yet to be described). This block then outputs the front and rear wheel angular velocities which are used by the tire forces block. The tire forces block also uses the vehicle velocity and normal forces on each tire to generate the tractive forces using governing equations of wheel dynamics. These normal forces are generated by the normal forces block, which implements the vehicle pitch due to acceleration and road grade integrated in the longitudinal vehicle dynamic equations. Finally, the longitudinal vehicle dynamic equations are implemented in the longitudinal dynamics block. This block uses the tractive forces and gravitational force acting in the longitudinal direction to generate the vehicle velocity and position.

The controller is then implemented in the lower half of the SIMULINK diagram. This controller can be removed and/or replaced if other testing is desired. This section can be described by following the flow from right to left. The first block on the lower right simulates the dynamics of the preceding vehicle. This block integrates a given preceding vehicle velocity profile. The controller inputs the range and range rate generated by the preceding vehicle block. If the controller is ACC then these are all the inputs, while CACC controller also inputs the signal communicated by the preceding vehicle. The controller has 2 levels. The upper level computes a desired vehicle acceleration using a free flow controller and an ACC or CACC controller (all to be described later). The lower level then tracks this desired acceleration using the throttle and brake actuators. The lower level also includes switching logic to prevent the application of the throttle and brakes at the same time, thus when accelerating the brakes are not applied while when decelerating the throttle is not running.

Vehicle model in HMC

In HMC, due to the large number of simulated components and the complication of the scenario, we use the simple longitudinal vehicle model in equation (2.1) to save computation load.

$$\begin{aligned} \ddot{x}(t) &= a(t) \\ \tau\dot{a}(t) + a(t) &= u(t) \end{aligned} \tag{2.1}$$

The model composed of a double integrator and a first-order lag, where $x(t)$ and $a(t)$ are respectively the position and acceleration, and $u(t)$ is the commanded acceleration from the controller. The flow of information among the simulation components is the following:

- Sensors output range and range-rate to the controller.
- Controller outputs acceleration command to the first-order lag.
- Lag outputs actual acceleration to vehicle dynamics.
- Dynamics integrates and outputs velocity.
- Velocities of all vehicles are integrated to update their positions, which can then be read again by sensors.

2.4.2 Controller Design

ACC Controller

The ACC controller is designed with the sliding surface technique in order to regulate the range error and range rate error.

The sliding surface is defined in equation (2.2).

$$S = (v_p - v) + \Lambda \cdot (r - r_{des}) \tag{2.2}$$

In (2.2) v_p and v are respectively the velocity of the preceding vehicle and the ACC/CACC vehicle, therefore $v_p - v$ is the range rate, or equivalently the relative velocity. r and r_{des} are the range and desired range, therefore the latter term in (2.2) is the range error to eliminate. The gain Λ is a design parameter which determines the speed of the convergence of range error to zero, once we are on sliding surface.

Instead of the commonly used time-gap model for the desired range, we use the desired range defined in equation (2.3), which is a curve fitting result of human driver behavior provided by the manufacturer of the OVC test vehicle [23].

$$r_d(t) = t_h * v^{k_0} + offset = 6.33 * v^{0.48} + 2 \tag{2.3}$$

We observe that the increasing rate of this desired range is smaller than the time-gap model when the velocity is high.

We derive the desired acceleration to drive the range error and range rate to the sliding surface, thus both to converge to zero with time. For this we need to have

$$\dot{S} = -K \cdot S \tag{2.4}$$

where K is also a design parameter which determines the decay speed of S.

Plugging (2.2) and (2.3) in (2.4) we obtain the ACC controller as in equation (2.5):

$$a_{des} = \frac{1}{1 + k_o t_h v^{k_o - 1}} \cdot [(\Lambda + K) \cdot \dot{r} + \Lambda \cdot K \cdot (r - r_d)] \tag{2.5}$$

In the equation $r(t)$ and $\dot{r}(t)$ are the range and range rate, and $r_d(t)$ is the desired range. The desired acceleration a_{des} is the control command, and $\Lambda + K$ and $\Lambda \cdot K$ are the controller gains. We observe the influences of Λ and K to the controller are symmetric. Gain scheduling is used to deal with different relation of the range and range rate. The rough rule is that for shorter range (closer to the predecessor), and more negative range rate (slower than preceding vehicle), the controller reacts more aggressively [23]. The absolute value of the acceleration commanded by the controller is a measure of control effort. For the same level of performance on range error and range rate responses, better controller design demands less control effort. The acceleration of the ACC/CACC controllers is bounded to be between -3m/s/s and 2m/s/s for safety and comfort purpose, but such limits do not apply to the human drivers (details in 2.4.4).

CACC Controller

When CACC scheme is applied, we change the desired range properly and use the same controller structure as in equation (2.5) to track this modified desired range. Both in the cut-in scenario of the OVC and the HMC, whenever a CACC vehicle receives a "relevant" message warning it of a vehicle cutting in front in t_{cut_in} time, it changes the desired range in the way described in (2.6).

$$\tilde{r_d} = \left[1 + \frac{(t - t_r)}{t_{cut\_in}}\right] * r_d + \frac{(t - t_r)}{t_{cut\_in}} * L \tag{2.6}$$

In the equation, r_d is the desired range defined in (2.3), $\tilde{r}_d$ is the modified desired range for the CACC controller, t_r is the instant of the reception of the warning message, t_{cut_in} is the estimated time left for the arrival of the cut-in vehicle, and L is the vehicle length. This modified desired range increases linearly in the time before cut-in/merging vehicle's arrival such that the CACC vehicle decelerates as aggressively as necessary without having to brake excessively hard. The desired range increases to twice as large as the original value, though the actual time response of the vehicle cannot really achieve this value at the end of transition.

In the braking scenario of OVC we interrupt the command of the ACC controller (2.2) and apply the smaller (larger in absolute value) of the ACC control command generated by (2.5) and the (negative) acceleration of the preceding vehicle, which is received from V-V communication.

Free-driving Controller

When a vehicle has no vehicle ahead of it or has at least 100 m of clearance to the preceding vehicle, the controller (of the automatic vehicle) is in the free driving mode. In this mode, the controller attempts to maintain a desired velocity, which was assigned when the vehicle entered the simulation. The distribution of desired velocity is taken from a normal distribution with a mean of 28.9 m/s (65 mph) and a standard deviation of 4.4 m/s (10 mph). Each type of controller uses an error-based control law:

$$u(t) = -k_f(v - v_d) \tag{2.7}$$

Where v and v_d are respectively the actual and desired velocity. In addition, acceleration is limited to $\pm 2m/s/s$.

The initial velocity of a newly generated vehicle, as it enters the simulation, is distributed in the same way as the desired velocity in free-driving state.

2.4.3 Communication Model

Two particular concepts of V-V/R-V communication are applied in our work. However seemingly simple, they help overcome many challenging problems in V-V/R-V communication on highway.

Location-based Broadcast

The first one is location-based broadcast (LBB) [45] [44], in which the sender broadcasts a message to all of the receivers in the communication range, and the physical location of the sender is written in the broadcast message. Each receiver determines the relevance of the message and the proper response by itself. Useful information for the sender in processing the message includes the relative physical position of itself to the sender (e.g. in front, behind, left lane, distance, etc.), the nature of the message (e.g. braking, lane changing, accident, congestion, etc.), and other information in the message (velocity, acceleration, etc.). By applying LBB we avoid the difficulty of network addressing and physical-location/communication-address mapping. The realization of LBB requires the interaction of wireless communication with other relevant techniques such as sensor fusion, GPS/INS, and digital map. It should be noticed that LBB is not suitable for all types of vehicle safety applications, and sometimes unicast is unavoidable.

Event-driven Communication

The other important concept underlying our implementation is event-driven communication. In this kind of communication, the transmission of a message is driven by particular events, e.g. cut-in, merging, hard braking of preceding vehicle, etc. Event-driven communication is in contrast to time-driven communication, in which vehicles transmit certain information (e.g. position, velocity, acceleration, road condition, etc.) to targeted receivers in every constant period of time (e.g. 100msec) [1] [43]. When large number of senders are competing for the channel, as is the case in V-V communication, event-driven communication reduces the load of channel and gives high priority to emergency message, thus simplifies the communication protocol design. Event-driven communication conveys less information than time-driven communication therefore is not sufficient for some applications. Our study helps find out which application can be supported by event-driven communication, and which application requires more complicated communication scheme. As we shall see below that the braking scenario in OVC is found to be an example where event-driven communication is insufficient.

2.4.4 Other Models in HMC

There are more models in HMC than in OVC since the former simulates much more complicated system. We describe them one-by-one below.

Highway Model

The highway is one lane and has limited access, with only passenger cars on it. Vehicles enter from left end at 0 m, and exit simulation at 700 m at the right end of the simulated highway segment. The merge-in point is at 500 m from the left end. In both lanes the vehicles are generated by an exponential distribution source with a given flow rate, which determines the time gap between two consecutive vehicles. The initial velocity is set as described in 2.4.2. The lateral motion of vehicles and geometry of merge-in ramp are not modelled, therefore in simulation the merging vehicles wait at 500 m after being generated, forming a queue sometimes, and pop in the main lane instantaneously when condition is satisfactory.

Sensors

Since by the time we conducted this work no generic model and parameters for sensor noise were available, we assumed all sensors to be perfect in the simulation. The simulations will be repeated with more realistic sensor model.

Braking Capabilities

In our simulation, hard braking is unlikely. However, to meet safety standards, our controllers must be able to handle such situations. We use a distribution of light vehicle braking capabilities from the NAHSC Task C3(1) Interim Report [5], assuming dry pavement. Engine braking is not modelled separately in HMC (unlike in OVC). Brake dynamics are not explicitly modelled, although the first-order lag applies to deceleration as well as to acceleration.

Human Driver Model

We use the COSMODRIVE model of Song-Delorme [40] because it has more room for tuning, and incorporates recent research on perception [25]. Human

drivers do not respond to the V-V/R-V communication messages.

Merging Model

We assume that merging is under human control in all cases, since automated control of merging is unlikely to be available in the near future. The human driver at the head of the merge queue waits until the gap between passing vehicles is of an acceptable length. When such a gap appears, the driver merges into it at the velocity of traffic. Our model for gap acceptance of human drivers is borrowed from the dissertation of K. Ahmed [6]. This model has been calibrated with driving data, and including it in our simulation produces realistic-looking traffic patterns. In this model, when seeing a good gap the driver of the merging vehicle is more likely to merge in, but the decision making model is probabilistic. A good gap cannot guarantee a merging, which also depends on other factors such as relative speed, perception delay, number of failed previous attempts, etc. In CACC, the relevant main lane vehicles try to make a more acceptable gap for the merging vehicle when the latter arrives, but it is (the model of) human driver, not any automated controller, who makes the decision of merging.

2.5 Simulation Results and Discussion

In this section we report and discuss the simulation results. The results for OVC and HMC are presented separately. The simulation system should be validated with experiment or measurement data of real world before any of the output data could be trusted. The validation of the OVC system was performed experimentally and reported in [23]. The validation of the HMC model will be presented shortly.

2.5.1 Results and Discussion of One Vehicle CACC Simulation

In OVC we compare the influence of ACC and CACC on the behavior of a single vehicle. We observe the performance of the vehicle in tracking the desired range and range rate, and the control effort with which to attain this tracking. In highway environment it is unusual for a vehicle to suddenly accelerate at a high rate, however there are many chances for a vehicle to

have to brake hard. Therefore the control effort concern focus much more on the braking behavior than on the (positive) accelerating behavior. The braking effort in this chapter refers to the absolute value of the negative acceleration. Since in the implementation of the vehicle model the brake and throttle are never applied at the same time, the negative acceleration of the vehicle is always due to the application of the brake. An optimal system should well track the desired range and range rate with as little as possible control effort, especially braking effort.

The range and velocity for cut-in scenario are shown in Figure 2.3. The velocity of the preceding vehicle remains to be 12.5 m/s in the simulation. At the beginning of simulation the follower (i.e. the CACC or ACC vehicle) is 150 meters behind the preceding vehicle and driving at 25 m/s. The follower brakes to track the preceding velocity. The cut-in happens at 10 second, making the range to drop instantaneously. The range after this instant becomes the range to the new preceding vehicle. For simplicity we set the cut-in vehicle's longitudinal velocity to be the same as the old receding vehicle. There is little difference on the range, though the velocity of CACC vehicle responds earlier than that of the ACC vehicle.

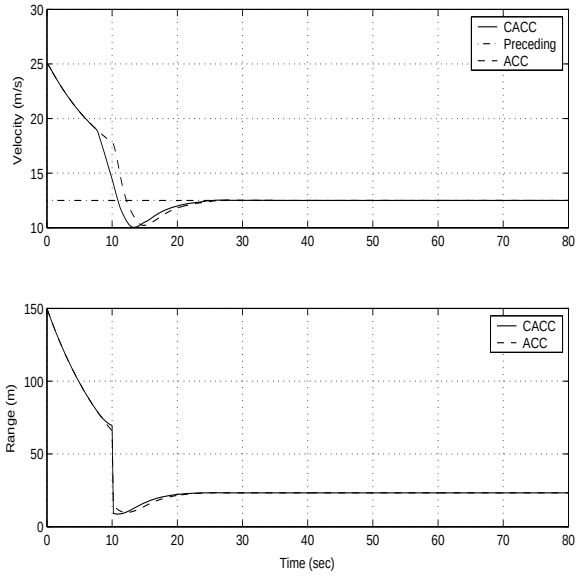

Figure 2.3: OVC: Range and velocity for ACC and CACC vehicles in cut-in scenario

Figures 2.4 and 2.5 are respectively the acceleration of the ACC vehicle and CACC vehicle in cut-in scenario. In both figures, the horizontal axis is time in second and vertical axis is acceleration in m/s/s. The cut-in happens at 10 second for both ACC and CACC cases. The ACC vehicle detects the cut-in vehicle shortly after 10 second, and then has to apply a hard brake of -2.5 m/s/s to slow down. After this hard brake, the velocity of the ACC vehicle decreases to a safe value. The acceleration thus goes back to the normal value, and finally converges to zero as the ACC goal is achieved. On the other hand, in Figure 2.5, because of the V-V communication, the CACC vehicle responds 2.5 seconds before the vehicle in the adjacent lane cuts in, which is half of the lane change time of the cut-in vehicle. Because the CACC vehicle has longer response time, it brakes much more softly than the ACC vehicle. The braking effort is smaller than 0.5 m/s/s, and the sharp notch shortly after 10 second in Figure 2.4 disappears. Combining the observation of Figures 2.3- 2.5, we see that the V-V communication saves large amount of control effort without sacrificing controller performance, which means more safety and comfort for the passenger.

Figure 2.6 is the range and velocity of the ACC/CACC controlled vehicle in the braking scenario of OVC. Here we use a preceding velocity profile collected by driving the test vehicle on street. We can see that CACC vehicle has a little faster time response than ACC vehicle, but the difference is not significant enough to draw any clear conclusion. The control effort comparison shows the same result, which we omit here to save space. The reason of this similarity in performance may be that the quality of the forward-looking sensor implemented in the simulation is high and the response time gained by addition of communication is not long enough for the vehicle to yield much difference in performance. The gain in response time is further trivialized after the command signal is filtered by the much slower vehicle dynamics to obtain the response in vehicle motion. From the simulation we build, it looks that event-driven communication does not help a lot in a scenario like the braking warning. The test with realistic sensor implementation is left for future work.

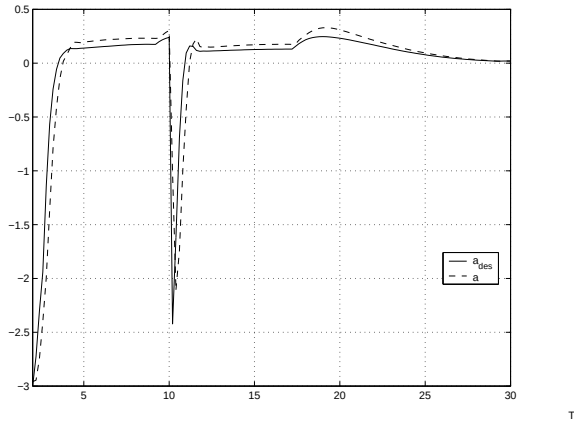

Figure 2.4: OVC: Acceleration of ACC vehicle in Cut-in Scenario

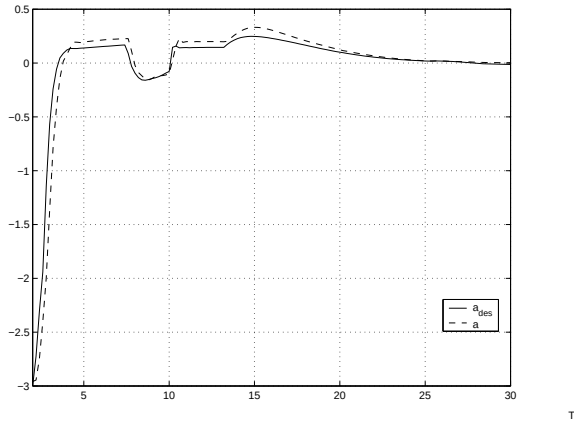

Figure 2.5: OVC: Acceleration of CACC vehicle in Cut-in Scenario

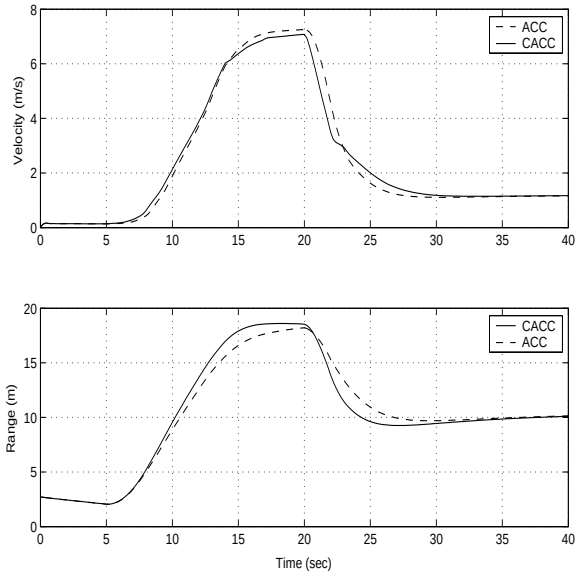

Figure 2.6: OVC: Range and velocity for ACC and CACC vehicles in braking scenario

2.5.2 Results and Discussions of Highway Merging Control Simulation

Having observed the effect of V-V communication in OVC, in particular the cut-in simulation, we are much motivated to conduct the study of HMC since highway merging is to much extent the macroscopic correspondence of cut-in.

In this subsection we first present results on the validation of the simulation system in 2.5.2, which shows the reliability of all the simulation results following. With the system validated, we study its performance with various design parameters. The performance variables, or with slight abuse of terminology, the dependent variables, are the following.

1. *Average Velocity of Main Lane Vehicles*

   The average velocity indicates the average trip time a vehicle spends on the simulated segment of highway, therefore a high average velocity for main lane vehicles means an efficient transportation system.

2. *Braking Effort of Main Lane Vehicles*

The maximum braking effort (the absolute value of the minimum negative acceleration) is used as the indication of the cost for the corresponding efficiency performance. The maximum braking effort tells us how hard a vehicle has to brake for the disturbance of the traffic. Too large braking effort is dangerous and sometime not achievable, and it also causes passenger discomfort. Since the only major disturbance for all main lane vehicles is the merging, the maximum braking for most vehicles is due directly or indirectly to the merging vehicles.

3. *Queue length of Waiting-to Merge Vehicles*

   The above two variables are those of the main lane vehicles. It is true that the main lane traffic should be disturbed as less as possible by the merging. However system design should not sacrifice the merging lane. Because as described in 2.4.4, we do not model the dynamics of merging vehicles or the geometry of the ramp, the only variable indicating the merging lane efficiency is the length of the queue of waiting vehicles. For the same input flow rate of main lane and merging lane, a good control system design shortens the queue.

We study the impact of the following three categories of independent variables on the dependent variables described above:

1. *ACC or CACC*

   It is equivalent to the indicator variable of system being with or without vehicle-vehicle/roadside-vehicle communication.

2. *Market Penetration of ACC/CACC Vehicles*

   A system with half of vehicles controlled by ACC certainly performs differently to a system with all vehicles being ACC. We observe this difference via simulation. A clarification which we have made above in 2.3.2 is that all through this chapter we never mix ACC with CACC vehicles. In the mixed cases the vehicles are composed of either ACC vehicles mixed with human drivers, or CACC vehicles mixed with human drivers. Whenever we say the mixed case of $X\%$ of ACC vehicles, by default there are $(100-X)\%$ human-driven vehicles. The same goes for CACC vehicles.

3. *Aggression of Controller*

As stated above the CACC controller uses the same control structures as the ACC controller, only that the CACC controller tracks a modified desired range when receiving a warning message from a "relevant" vehicle. Therefore obviously the aggression of the controller (2.5) plays a critical role in determining the time-response characteristics and the control effort in both systems. We adjust the controller gains $\Lambda + K$ and $\Lambda \cdot K$ in equation (2.5) and compare the performance of the system with strong gains to that of the system with weak gains.

We discuss the results for average velocity of main lane vehicles in 2.5.2. Results of main lane vehicles' braking effort are shown in 2.5.2. In 2.5.2 we show some results regarding the shock wave generated by the merging in the main lane vehicles, which contributes to the statistics of average velocity and braking effort in 2.5.2 and 2.5.2. Finally in 2.5.2 we discuss results of the merging queue length.

System Validation

Before using simulation output to study ACC/CACC controller design, we should first validate that the simulation system itself is a good representation of the real physical system. The modeling should provide a representation of the real world which is simple enough to make the problem tractable, while not too simple such that any essential components are lost.

As described above, all of the models we applied in the over-all simulation system are taken from published work, each being well analyzed and validated individually or directly from measurement, e.g. the human driver model (2.4.4), the gap acceptance model (2.4.4), and the braking capability distribution (2.4.4). However never before were they integrated to form one system to simulate all aspects of the highway behavior. Therefore before conducting any simulation, we need to first validate the overall system.

We run the simulation in the "all-human" scenario, i.e. all automated control components (ACC or CACC) are turned off. The system is thus no more than a simulation of regular highway segment. We compare the simulated results with the measurement data of real highway taken from the Freeway Performance Measurement System (PeMS) [3]. PeMS is a collaborated project of the Department of Transportation of California, University of California at Berkeley, and California PATH. The PeMS system collects the real-time measurement data of major highways in California with loop

detectors and stores it in database. The measurement data we use here is randomly taken from one lane of highway I-80E at sensor 313111, which is located in city of Sacramento, on the day March 15, 2003. We compare the flow-density (Q-K) relations of the two sets of data in Figure 2.7. Based on the argument of [22], we perform two-portion linear fitting on the data, with the left portion representing the uncongested flow-density relation while the right portion representing the relation in the queues formed on highway (compare with Figure 4 of [22]). Since there is not an freeway exit in our simulation besides the end point at 700 meters, we cannot observe the "queue discharged" Q-K relation in Figure 4 of [22]. The results show that the simulation data is quite close to the measurement data. They both obey the two-portion linear model, and the maximizing density values are quite close. The result shows that the overall simulation system is a pretty reliable tool to study the behavior of the highway traffic.

The error could come from any component of our model, and from our ignorance of lane-changing — we use the data of one lane of the I-80E instead of the data of a one-lane highway. The detailed analysis of the source of the errors and the calibration of the model to further reduce the error are left as the future work.

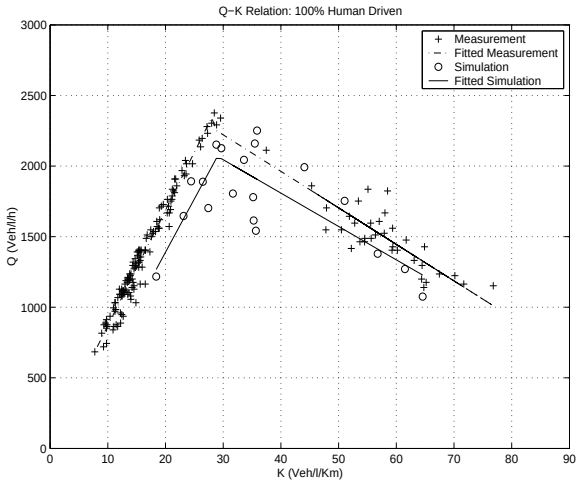

Figure 2.7: System Validation for HMC: Comparison of simulation data with measurement data from PeMS

Having validated the system, we now study the performance of the HMC. In all the following subsections, the initial conditions are the same. The input

flow rate for the main lane is 2000 vehicles/lane/hour and the flow for the merge lane is 600 vehicle/lane/hour, and the initial velocity of the main lane vehicles are assigned as described in subsection 2.4.2. We simulate the system for long enough time for 30 minutes trip time of vehicles, thus typically more than 1,000 vehicles appear in the main lane. This assures that the statistics we present below are significant.

Average Velocity for Main Lane Vehicles

In Figure 2.8, we compare the average velocity performance for four cases: CACC system with strong controller, CACC system with weak controller, ACC system with strong controller, and ACC system with weak controller. We expect to observe the role played by V-V/R-V communication as well as by controller aggressiveness in this set of results. As described in 2.4.2 that the ACC and CACC controller have the same structure and the difference lies in the desired range, thus in this section when we say CACC system with strong controller and ACC system with strong controller, the control gains are the same, so is true for weak controller.

The system simulated in Figure 2.8 has 100% market penetration of controlled vehicles (i.e. 100% CACC vehicles if the system is CACC and 100% ACC vehicles if the system is ACC). The Figure shows the cumulative probability distribution function of the average velocity, therefore the y-value is the portion of vehicles with average velocity lower than abscissa. We observe clearly that in term of average velocity, strong controller performs better than weak controller (given that both are ACC or both are CACC), and for the same controller aggressiveness CACC system outperforms ACC system. For instance, the percentage of vehicles with average velocity smaller than 15 m/s is respectively about 10%, 25%, 40%, and 58% for CACC with strong controller, ACC with strong controller, CACC with weak controller, and ACC with weak controller.

CACC system performs better than ACC system due to the benefit of communication. With V-V/R-V communication the main lane vehicles know about the merging in advance, therefore the relevant vehicle brakes smoothly in longer response time. Its followers also have a smoothed brake period and their average velocity do not suffer so much from the merging disturbance as in the system where vehicles do not prepare for the merging. Strong controller respond more promptly to the disturbance than weaker controller. Therefore the more aggressively controlled vehicles are disturbed for shorter

time, and disturbance propagate to less of its following vehicle. The system-wide behavior of average velocity does not suffer so much as when weaker controller is applied.

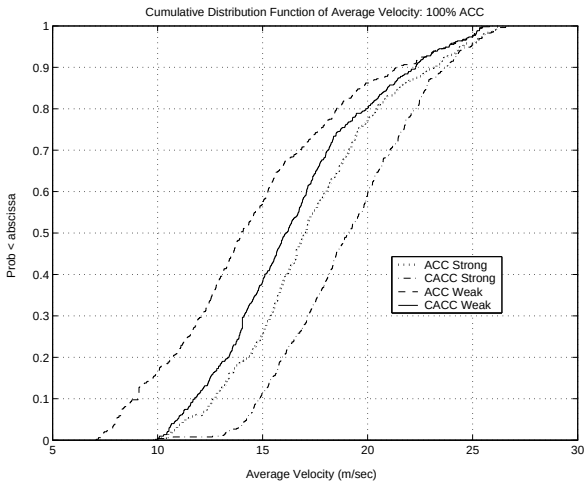

Figure 2.8: HMC: CDF of Average Velocity (Market Penetration = 100%)

Figure 2.9 is the empirical cumulative distribution function of the average velocity for different market penetration of CACC. It is evident that the curves for higher percentage of CACC vehicles lie below the curves for lower percentage. This means that lower percentage case has more vehicles running with average velocity lower than a given value. For example, when 20% of all vehicles are CACC, there are about 60% vehicles having average velocity lower than 10 m/s, while almost no vehicle drives slower than 10 m/s if all of the vehicles are CACC (100% curve). The highest velocity in all cases shown is close to about 28m/s. This is because a vehicle generally has highest velocity possible when it enters the simulation, where we set the initial velocity to around 28.9 m/s (See subsection 2.4.2). For some lucky vehicles the average velocity is about the same as the initial velocity, but most vehicles have to slow down once they are in the highway segment because of the merging disturbance. Similar effects of market penetration is observed in the ACC system. These results tell us that system with higher market penetration of controlled vehicle benefits all vehicles on highway by saving trip time. The result seems natural since with higher percentage of controlled vehicle, the beneficial impact brought by ACC or CACC is larger.

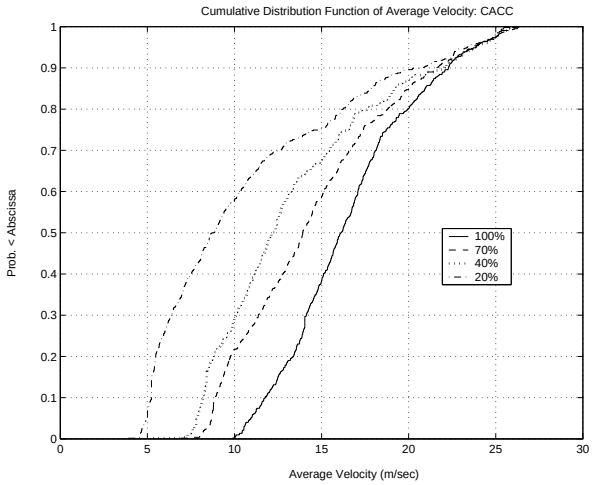

Figure 2.9: HMC: CDF of Average Velocity of CACC vehicles

Maximum Braking Effort of Main Lane Vehicles

Figure 2.10 compares the same four cases as in Figures 2.8, but focusing on the maximum braking effort, i.e. the minimum negative acceleration exerted by a vehicle in the duration of simulation. Shown here are the CDF's of the maximum braking effort. Observation is that for given controller, integration of V-V/R-V communication saves braking effort, while for a given system (either with or without communication), weak controller utilizes less braking effort than strong controller (except for some small braking effort values). For example, the percentage of vehicles executing maximum braking effort larger than 1.5 m/s/s (minimum negative acceleration smaller than -1.5 m/s/s) is approximately 8%, 20%, 30%, and 50% for CACC with weak controller, ACC with weak controller, CACC with strong controller, and ACC with strong controller.

Figure 2.11 shows the empirical CDF of maximum braking effort for different market penetration of CACC vehicles. It could be regarded as the cost of the efficiency performance shown in Figures 2.9. We can see that the more controlled vehicles mixed in the traffic, the more braking efforts are saved. This can be observed as curves for higher percentage cases are blow the curves for lower percentage cases. For example, in 20% CACC vehicle case, more than 85% of all vehicles have maximum braking effort larger than 1 m/s/s (minimum negative acceleration smaller than -1 m/s/s), while only

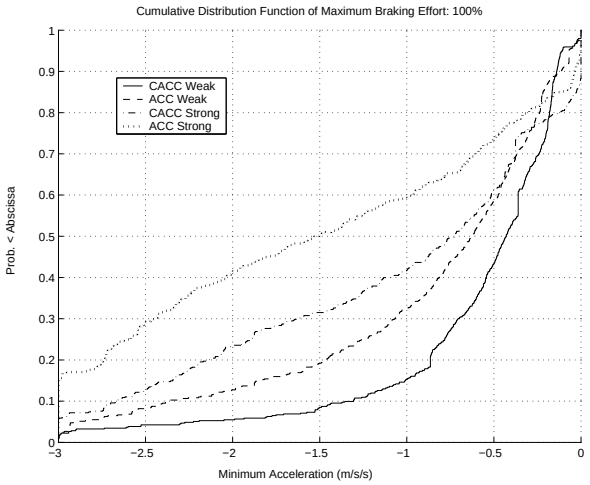

Figure 2.10: HMC: CDF of Maximum Braking Effort (Market Penetration = 100%)

about 40% vehicles experience maximum braking effort larger than this value when 100% of vehicles are CACC. Similar influence of market penetration is observed for ACC system. Combining these results with those shown in Figure 2.9, we conclude that higher market penetration of ACC/CACC vehicle always brings advantage over lower market penetration in both the "gain" and the "cost".

Figure 2.12 shows the average maximum braking effort vs. percentage of controlled vehicle for various cases. The former value is obtained by averaging the maximum braking effort of all main lane vehicles appeared in the simulation. In all the cases presented here, whenever we say the market penetration of ACC is X%, the other 1-X% vehicles in highway is human-driven. The same goes for CACC system. Evidently, for both ACC and CACC systems, the higher the market penetration the smaller the average braking effort. With the same percentage of controlled vehicle, CACC system spends less braking effort than ACC system. Also for the same market penetration, either in a CACC system or ACC system, a weak controller saves control effort over a strong controller.

Communication makes the CACC vehicle aware of the merging in advance, therefore the irrelevant vehicles could ignore the merging vehicle and the relevant vehicle could brake smoothly in longer response time. The chance of abrupt braking is decreased, and the all the following vehicles

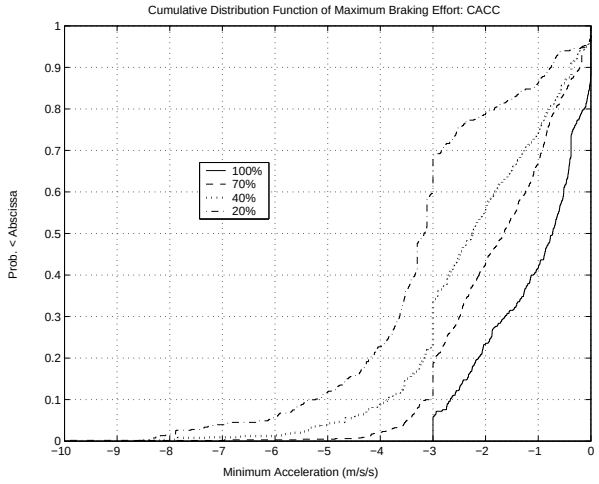

Figure 2.11: HMC: CDF of Maximum Braking Effort of CACC vehicles

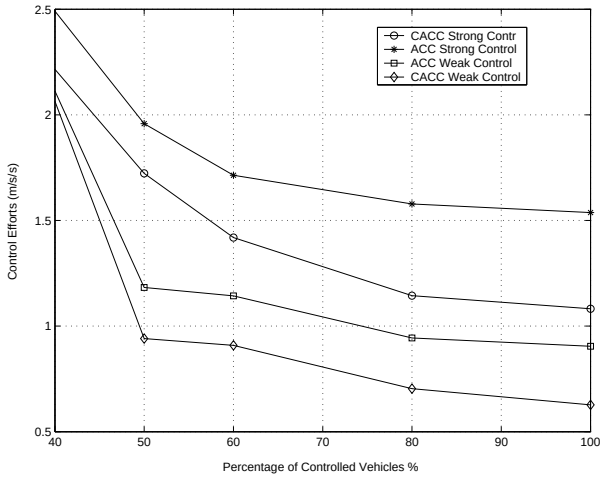

Figure 2.12: HMC: Average Maximum Braking Effort

brake less hard than in the scenario without communication. The result shown here agrees with the microscopic results shown in subsection 2.5.1. Combining the results shown in Figures 2.8, 2.10, and 2.12, we can see that communication makes the highway traffic more efficient with lower cost.

For a given disturbance a stronger controller responds more aggressively, sometime over-responds. Therefore although it makes the system respond faster to the disturbance thus less disturbed, as shown in Figure 2.8, this benefit is not gained without cost. Hence we have a tradeoff here. On one hand we have efficiency, and on the other we have safety and passenger comfort. We leave as a future work the design of controller achieving optimal relationship between these two aspects. One should also notice that, even considering only the efficiency, strong controller cannot achieve too much. For example, the average velocity cannot keep increasing as we use stronger controllers. This is because the vehicle can never apply acceleration over the saturated limits (see 2.4.2), and can never respond faster than what the vehicle mechanical dynamics is capable of.

We are aware that one cannot easily draw conclusion about the comparison between the CACC with weak controller and ACC with strong controller cases, although the former performs better in the particular tests shown here. The rigorous comparison between these two cases requires the precise definition of controller aggression and other sets of test which are not the focus of this chapter. The aim of the discussion here is to compare the effect of controller aggression with the system being either CACC or ACC, and the influence of the V-V/R-V communication on the system given a certain controller.

Trajectories of Main Lane Vehicles and Shock Wave

Figures 2.13 and 2.14 are the trajectories of vehicles in the main lane between 900 second and 1000 second for ACC and CACC HMC simulation. The horizontal axis is time in second and the vertical axis is the position of the vehicles relative to the starting point of the simulation in meters. Each curve corresponds to the trajectory of one vehicle. The merge-in point is at 500 meters. The horizontal line at 500 meter represents queued merging vehicles. Merging vehicles can be identified by a curve which lies entirely above this line. In both of these two figures we have 100% controlled vehicles on highway. We can see clearly in Figure 2.13 a shock wave propagating upward the traffic flow, i.e. in the opposite direction of the traffic. From about 910 second to

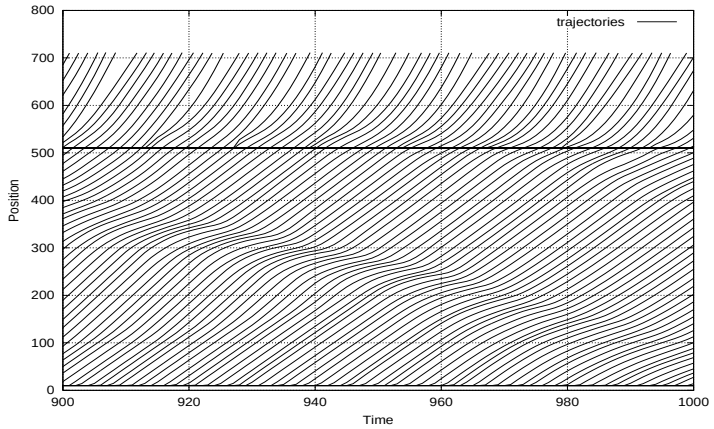

Figure 2.13: HMC: Trajectories of ACC Vehicles

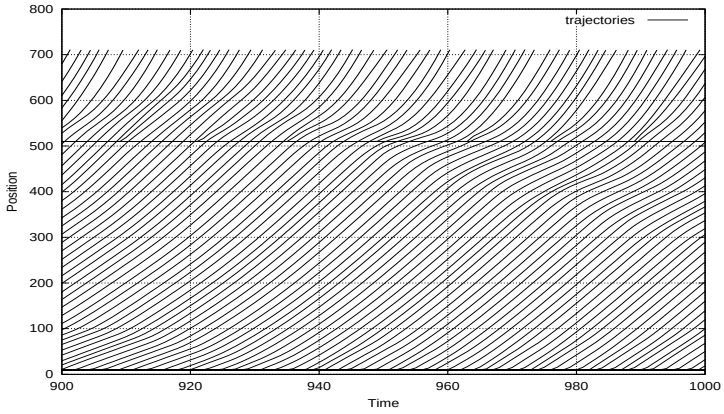

Figure 2.14: HMC: Trajectories of CACC Vehicles

970 second each vehicle travelling between approximately 150-350 meters has to apply a brake to slow down due to an earlier merging vehicle. All the vehicles lies in the wave are clustered together with much smaller range than in usual situation. About 10 seconds later the system recovers and vehicles speed up to usual velocity, and the shock wave propagates upstream until finally being damped off at around 970 second. However this shock wave is smoothed in Figure 2.14. Notice that the initial conditions for simulations are the same for the two cases. This type of phenomena is common in our simulation results. It confirms the advantage of CACC system over ACC system in terms of average velocity and braking effort. The reason lies in two facts. First is that in CACC system the relevant main lane vehicle receives the warning message, thus it can brake smoothly to increase the gap to the preceding vehicle. Second is when the merging vehicle enters the main lane, the gap it is in is already large enough for safety, and the main lane vehicles behind it do not need to brake hard, as they sometime have to do in ACC system.

Queu

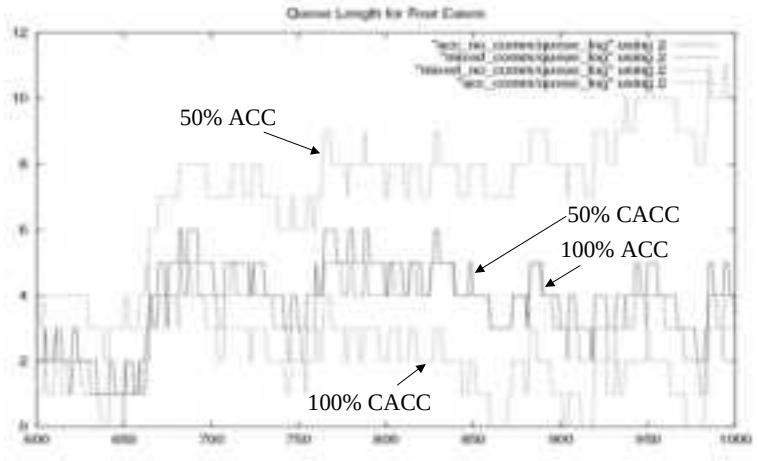

Figure 2.15: HMC: Queue Length of Waiting-to-merge Vehicles

Figure 2.15 shows the length of the queue of the waiting vehicles in the merge-in lane from 600 to 1000 second. Results for four cases are plotted here. The top curve is for 50% ACC main lane vehicles. In the middle, two

curves standing for 100% ACC and 50% CACC are quite close to each other. The bottom curve is for 100% CACC. The queue length keeps increasing because we intentionally inject a large flow rate of the entering vehicles to observe the system performance in critical cases. Clearly, system with larger percentage of ACC (CACC) vehicles has shorter waiting queue. For the same percentage, the queue in CACC highway is up to 5 vehicles shorter than in ACC highway. Due to the communication, the relevant main lane vehicles have longer time to make a good gap in front. By the time the merging vehicle arrives at MP, it is more likely to see an acceptable gap and merge in than reject the gap and wait. Therefore in average the merging cars wait for shorter time in CACC highway.

Chapter 3

Vehicle-vehicle Communication Protocol Design

3.1 Introduction

Vehicles on highway require a short to medium range communications service that supports both public safety and private operations in roadside to vehicle and vehicle to vehicle communication environments. This kind of communication service is meant to be a complement to cellular communications by providing very high data transfer rates in circumstances where minimizing latency in the communication link and isolating relatively small communication zones are important.

A spectrum of 75 MHz width at 5.9 GHz was newly assigned by Federal Communication Commission (FCC) to DSRC. This new spectrum allows the US, Canadian, and Mexican Intelligent Transportation Systems (ITS) programs to evolve to a new generation of RF communications between vehicles and the roadside, and among vehicles, that enables a whole new class of communications and a new class of applications to support future transportation systems and needs. The North America DSRC standard program is formed to develop a set of DSRC standards that will support full interoperatability throughout North America while satisfying all of the application requirements [1]. In this project, we designed and analyzed the first communication protocol that could be used by the safety applications for highway vehicles which follows the regulations of DSRC standard.

The allocation of DSRC is recent and the standardization process is not

finished, therefore relevant literature is rare. However the application of wireless communication and network techniques in the control of the vehicles and highway traffic has attracted much interest both in the field of communication as well as transportation study. Literature shows attempts on channel modeling [27], cooperative adaptive cruise control [43] [44], Automated Highway Systems [24], and wireless vehicle network [10]. DSRC is the first standard enabling technique to support all these work in long term.

The rest part of the chapter is structured like the following. Section 3.2 introduces the concept of location based broadcast (LBB) and discusses its importance in vehicle-vehicle communication. Section 3.3 describes a LBB protocol we design and analyze in this work. Section 3.4 summarizes the analytical results we obtained for the performance of the protocol, although we do not provide much detail of the analysis sue to space limit. Section 3.5 is the sensitivity analysis of the protocol to critical parameters in vehicle-vehicle communication system.

3.2 location based broadcast and unicast

In the most general sense, the vehicle-vehicle communication in DSRC could be classified as Location-Based Broadcast LBB and unicast. Our work is focused on the design and analysis of LBB protocols.

In Location Based Broadcast [44], sender broadcasts messages to all receivers in its communication range. It is the receiver's responsibility to determine the relevance of message and the proper response. The decision is made on basis of the relative position of the sender (e.g. in front, behind, left lane, distance, etc.), the purpose of the message(e.g. brake warning, lane change warning, accident reporting, congestion prediction, etc.), as well as the highway traffic environment. In DSRC the LBB protocol is built on top of IEEE 802.11a broadcast mode, since 802.11a has been selected by the DSRC standard committee as the MAC layer protocol. To realize LBB, wireless communication techniques must be integrated with other techniques such as Global Positioning System, Inertial Navigation System, digital map, radar, and sensor fusion. The LBB is the enabling technique for wide range of highway safety applications such as cooperative collision warning and emergency vehicle warning.

The realization of unicast vehicle-vehicle communication also requires the assistance of LBB. In order to establish initial vehicle-vehicle unicast commu-

nication, we must solve the anonymity problem in ad hoc vehicle communication networks, i.e. the communication addresses of vehicles on highway are unknown to each other at the beginning. Location Based Addressing (LBA) is needed to build (in all involved vehicles) the map between the physical location of surrounding vehicles and their communication addresses. This map basically answers the question "What is the communication address(es) of the vehicle(s) at given position(s)?". LBB is essential for the realization of LBA. This is because that the LBA process depends on the vehicle-vehicle communication, while only broadcast communication is available before the addressing is accomplished. Furthermore, the address-position map must be updated at proper frequency because of the dynamic property of vehicle communication network. This update process also has to rely on LBB since when update is necessary, the configuration of unicast network may already have changed and thus unreliable. Except for the building and updating of LBA map, the unicast vehicle-vehicle communication system is not fundamentally different from standard unicast communication system, and many established techniques could be applied.

Therefore to design a communication protocol to realize LBB that satisfies the requirements of highway safety applications is one of the most important tasks in the design of DSRC system. In this project we aim to provide a first attempt in solving this problem.

3.3 A location based broadcast protocol based on repetition coding

3.3.1 An Example of Highway Safety Application

The primary goal of the vehicle-vehicle communication protocol we consider is to support vehicle safety application, therefore it is necessary for us to understand the communication requirement of the safety application before designing the protocol. The following is an example application.

Cooperative Collision Warning [28]:

1. Definition

   Use vehicle-to-vehicle communication to collect surrounding vehicle locations and dynamics and warn the driver when a collision is likely.

2. Application needs

   (a) Communication from vehicle to vehicle

   (b) Two-way communication

   (c) Point-to-multipoint communication

   (d) Allowable latency $\sim$ 20–200 msec

   (e) Frequency (update rate) $\sim$ 10 Hz

   (f) Data to be transmitted and/or received - position, velocity, acceleration, heading, yaw-rate

   (g) Range of communication $\sim$ 50–300 m

The primary task of the DSRC communication protocols we consider here is to support such safety application. It can be seen that the system has to communicate small amount of information consistently at high frequency, with low delay, and competing with many transmitters. We describe our proposed protocol to meet these challenges below.

3.3.2 The LBB Protocol

The protocol we propose works as following.

1. Vehicle safety applications generate a message to be transmitted to other vehicles when an event (e.g. braking, emergency) occurs. The safety application's requirements provide a useful lifetime of the message. For example, after 100 msec from the braking, a brake warning message may be regarded as out of date and useless to the collision avoidance applications of other vehicles. We denote the useful lifetime as τ. The protocol attempts to transmit the packet only within the message's lifetime and discards the packet when the message has expired.

2. The information in the *message* is encapsulated in a lower layer *packet* to be transmitted to other vehicles. The packet could contain the location of the sender, the targeted vehicle's location (e.g. the first following vehicle, all vehicles in the adjacent lane), the nature of the event (hard braking, accident, severe road condition), etc. The time taken to transmit one packet is a function of the packet size and the channel bit rate. We denote this time period as t_{trans}.

3. The whole lifetime is evenly divided into $m = \lfloor \frac{\tau}{t_{trans}} \rfloor$ slots. The fraction of τ that is not used is quite small since in general $\tau \gg t_{trans}$ (τ is in the order of millisecond or even second while t_{trans} is in the order of microsecond. See below for detail).

4. In each of the slot, the protocol determines wether to transmit a packet in this slot by flipping an unfair coin with $P(H) = \frac{n}{m}$ and $P(T) = 1 - \frac{n}{m}$. A packet is transmitted if a head is obtained, where $n < m$ is an integer, which is the design parameter of the protocol.

5. If any one or more *packets* are transmitted without being collided, the *message* is received by all the vehicles in its communication range, and the delay is smaller than the useful lifetime of the message. On the other hand, the message transmission fails if all its transmitted packets are lost due to collisions. In this first-shot analysis we assume all transmitters have common clock therefore all the slots of various transmitters are synchronized.

Figure 3.1 is a illustration of the protocol. Two vehicles within interference range of each other have messages generated at same time, and the protocol makes them choose multiple slots to transmit a packet in each. Some packets collide but as long as there is at least one packet goes through the transmission is successful. Both vehicles in the figure succeed if there are no other interfering vehicles.

In the analysis below we assume that the value of n is the same for all vehicles, i.e. all vehicles have the same protocol design. From the law of large number we can see that in average each vehicle transmits the packet of one message n times, although the exact transmission number for each one particular message varies. Our protocol is therefore essentially based on repetition coding. Intuitively, repetition enhances the probability for at least one packet to get through over when transmitting only once. However excessive repetitions add burden to the channel and degrade the performance. Therefore the optimal number of transmissions n_{opt} must be found.

The protocol we proposed is relatively simple. In this first shot analysis, the LBB protocol does not "listen before transmission", and the receivers do not acknowledge the receipts. However the design and analysis of the simple protocol could provide us with insight at least in the following three aspects. Firstly, we could obtain the worst bound of the performance of smarter protocols built on basis of the study of the current one. Secondly,

we could find which applications could be supported by the simple protocol and which require more complicated protocols. Lastly, we could find out which parameters have significant effects on the performance.

3.4 Analysis of the protocol

There are two communication requirements on the performance of the protocol.

- *Channel occupancy caused by the vehicle-vehicle communication must be low.* Applications should not take too much of the channel time, such that the potentially large number of transmitters in highway environment can be accommodated (e.g. in the congested highway), and multiple safety applications could be working simultaneously.
- *The probability of failure for message transmission must be low.* With large number of transmissions in the same channel and each transmitting frequently, just as in highway environment, packet collisions happen quite often. However low failure probability is critical for the safety application. A good protocol should perform well in this aspect.

3.4.1 Probability of Failure

We make the following two assumptions to analyze the performance of protocol in prob

- The me s a Poisson process

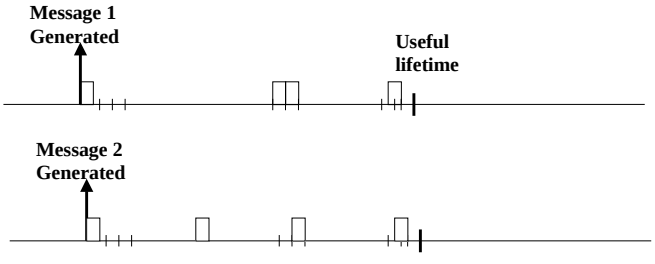

Figure 3.1: The LBB Protocol

- The message generattion processes of different vehicles are identically independent.

With these two assumptions, we know immediately that the generation process of all messages is also Poisson with the rate equal to the sum of the rates of all transmitters in interference range. Assume that the rate of the Poisson process for each transmitter is λ' then the generation process of all the messages is $\lambda =$ (transmitter number) * λ'.

Theorem 1 *The probability of failure P_f for one message satisfies the following inequality:*

$$\left(1 - \frac{n}{m} + q\frac{n}{m}\right)^m < P_f < \left(1 - \frac{n}{m} + p\frac{n}{m}\right)^m$$

where,

$$p = (1 - e^{-\lambda\tau\frac{n}{m}} + e^{-\lambda\tau})$$

$$q = (1 - e^{-\lambda\tau\frac{n}{m}})$$

e is exponential base
λ is the message generation rate for all transmitters
τ is the useful lifetime
m is the total number of slots in the useful lifetime
n is the average number of transmitted packet *for each* message

3.4.2 Channel Occupancy

We use equation (3.1) as the expression of the upper-bound of the channel occupancy, i.e. the average faction of time used to transmit all the message in the channel.

$$Occupancy = \lambda * t_{trans} * n \tag{3.1}$$

where as stated above λ is the generation rate of all messages, t_{trans} is the time taken to transmit one packet, and n is the average number of transmitted packet for each message.

The actual channel occupancy is smaller than this value since packet collisions are not considered here. Multiple packets that collide are all counted as occupying the channel in (3.1), although they overlap in time therefore their

effects are the same as one packet occupying the channel. If the channel occupancy calculated with (3.1) is satisfactory then the real channel occupancy can only be lower.

3.4.3 Performance of the Protocol: An Example

Figures 3.2 and 3.3 shows the analytical performance of the protocol with the parameters set as in Table 3.1. This is a typical setting for the parameters for a non-congested highway environment. The description and discussion of the parameters are in subsection 3.5.1.

In Figure 3.2, the horizontal axis is the value of n, and the vertical axis is the corresponding probability of failure calculated based on the upper-bound part of Theorem 1. We could observe that the probability of failure decreases with n at the beginning, and reaches a minimum value at about $n_{opt} = 23$, which is the optimal number of transmission in the sense of probability of failure. As n becomes larger after this value the probability goes up, so the performance degrades. This observation agrees with intuition. Figure 3.3 is the probability of failure vs. various channel occupancy, where channel occupancy is calculated with equation (3.1). We know that the (upper bound of) channel occupancy calculated here increases with n linearly, while the probability of failure decreases with n for $n < n_{opt}$, hence we could observe the trend of probability of error with increasing channel occupancy. We do not plot channel occupancy for $n > n_{opt}$ since with these values of n more channel is occupied without decreasing the probability of failure. In Figure 3.3 the channel occupancy for 0.001 probability of failure is about 50% (number of transmissions about 10). This performance of the protocol is satisfactory since about half of the channel time is left for other applications while the probability of failure is reasonably low. Also we see that as the probability of failure decreases more and more slowly as channel occupancy gets large. Thus after some point the gain in probability of failure by occupying more channel is trivial.

Table 3.1: Parameters of the Analysis Example

Message Generation Interval (msec)	100
Packet Size (Bytes)	200
Channel Bit Rate (Mbps)	10
Interference Range (m)	100
Average Distance Between Vehicles (m)	30
Lane Number	10

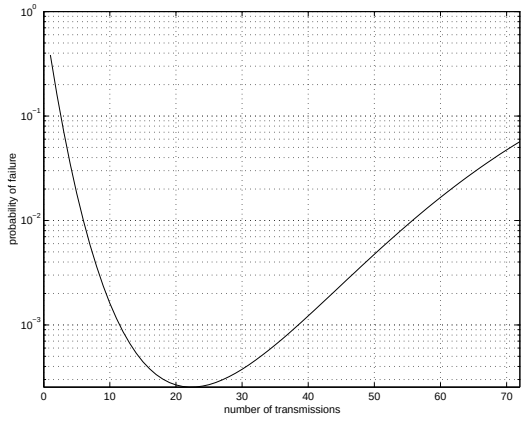

Figure 3.2: Probability of failure vs. Number of Transmission

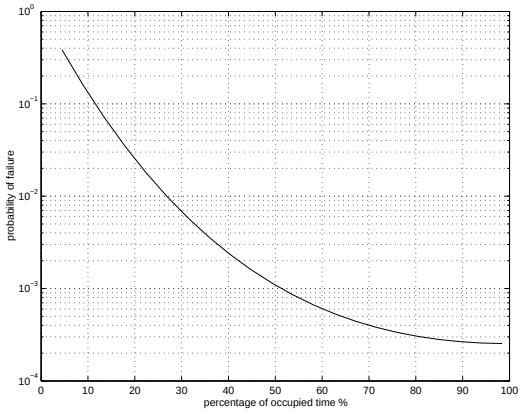

Figure 3.3: Probability of Failure vs. Channel Occupancy

3.5 Sensitivity test of the protocol under various environment

3.5.1 Determining Parameters of the Vehicle-vehicle Communication Performance

The parameters determining the performance of the LBB communication are the following:

1. *Message Generation Rate/Interval*

   They parameterize the frequency at which a safety application message is generated, therefore influence both probability of failure and channel occupancy. The message generation rate is the reciprocal of message generation interval. The actual message generation rate required comes from the specific safety application. We study what rate is supportable by our protocol.

2. *Packet Size*

   This parameter determines the channel occupancy. For vehicle safety application the packet size is generally not large, and is in the order of a few hundred bytes [1]. This comes from the fact that in most cases the information needs to be transmitted is the instantaneous position, velocity, acceleration, yaw rate, direction, warning, etc. All of these

could be represented by a few integers. Although the packet size is small, the potentially large number of interfering vehicles and the high transmission frequency makes the performance sensitive to the packet size.

3. *Channel Bit Rate*

   The channel bit rate together with the packet size determines the time taken to transmit one packet, therefore influences the channel occupancy. The channel bit rate we use here is 10 Mbps, which is determined from the proposed DSRC standard [1].

4. *Interference Range*

   This is the range that one vehicle's transmitted signal could be interfere with other vehicles. It affects both the probability of failure and channel occupancy by determining the number of interfering vehicles. Interference range itself is determined by the transmission power and the channel model. Instead of designing the power to transmit and modeling the channel we assume directly the resulting interference range, and the actual transmit power could be calculated from the interference range once we have the channel model and the interference threshold of the specific radio. The channel modeling of DSRC band in highway environment is an on-going work of the authors [4]. In the sensitivity study we assume omni-directional antennae, therefore the interference zone of a vehicle is a circle centered at the position of its antenna with the interference range as radius.

5. *Vehicle Density/Distance*

   The vehicle density is the reciprocal of the distance between two neighboring vehicles in the same lane. Once we know this value and the interference range we could calculate the total number of interfering vehicles for an individual vehicle, which influences both the probability of failure and the channel occupancy. Here we make an assumption that the traffic is at steady state in which all the vehicles have same constant distance from its neighboring vehicle in the same lane.

6. *Lane Number*

   When the transmission power is such that the interference zone overs all of the lanes in the direction perpendicular to the driving direction,

the lane number influences the number of competing vehicles in the interference zone. The lane width we use is 3.6 meters [35]. We test our protocol in some pretty severe circumstance, including the cases where the highway has 20 lanes, e.g. when there are multiple highway bridges overhead.

3.5.2 Results of Sensitivity Test

We conduct sensitivity test of the protocol with the parameters listed in Table 3.2. Wide range of parameters are tested to evaluate the performance of the protocol under various environment and the effects of different parameter to the performance are compared. Both jammed and smooth traffic cases are assessed.

Figure 3.4 shows the result of the sensitivity test for jammed traffic cases. Plotted here are the bounds of feasible parameter combinations that achieve the following two communication requirements:

1. Probability of Failure smaller than 0.01
2. Channel Occupancy lower than 50%

For example, the dashed-cube curve is for the case when there are 20 lanes and the packet size is 200 bytes. The data indicates that if the interference range is 20 meters, i.e. 2 vehicles in front and two in back in the same lane are covered, then the minimum message generate interval is 200 msec, i.e. 5 messages per second. It is impossible to transmit at higher rate with such interference range, without violating the communication requirements. On this same curve we observe that when the interference range is larger than 40 meters, no message generate interval we tested ($50 \sim 500$ msec) could achieve the two communication requirements. The area under the curve is infeasible while the area above it is feasible for the communication requirement. That means, given the interference range, the message generation interval values could not be smaller than corresponding values on the curve, and given message generation interval, the interference range cannot be larger than the corresponding value on the curve. Otherwise the communication requirements cannot both be met. We see that when the environment is less severe the feasible area is larger. For example, the feasible area for "100 bytes, 10 lanes" case is larger than "200 bytes, 20 lanes" case.

Table 3.2: Parameters of Sensitivity Analysis

Message Generation Interval (msec)	50, 100, 200, 300, 400, 500	
Packet Size (Bytes)	100, 200	
Channel Bit Rate (Mbps)	10	
Average Distance Between Vehicles (m)	7 (jammed)	30 (smooth)
Interference Range (m)	7-70	30-300
Lane Number	10, 20	

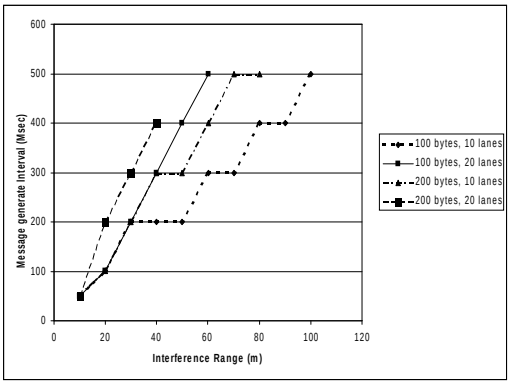

Figure 3.4: Sensitivity Test Results: Jammed Highway, Probability of Failure ≤ 0.01, Channel Occupancy $\leq 50\%$

Chapter 4

Slip-based Road Condition Estimation

4.1 Introduction

Many reports have introduced an algorithm to determine the road's frictional characteristics. However, this research focuses on obtaining the maximum braking performance of a car by using the maximum friction coefficient, μ_{max}, which can be estimated using the slip of a wheel. In other words, given the current road condition, it is important to know which way and how fast a car can be stopped without vehicle skidily. One easy way to determine when vehicle skid occurs is to calculate the maximum friction coefficient. The μ_{max} between the road and the tire can be obtained using Equation 4.1.

$$\mu = \frac{\sqrt{F_x^2 + F_y^2}}{N_z} \tag{4.1}$$

The F_x, F_y, N_z in this equation are longitudinal, lateral, normal force applied on the tire, respectively. In this report, F_y can be disregarded since only the longitudinal motion of a vehicle is considered, and lateral motion has been ignored. Therefore, Equation 4.1 can be simplified as shown in Equation 4.2

$$\mu = \frac{F_x}{N_z} \tag{4.2}$$

In Equation 4.2, the maximum friction coefficient is $\mu_{max} = \max|\mu| =$

$\max|\frac{F_x}{N_z}|$. Therefore, the normal force and maximum longitudinal force applied to a tire are known, the maximum friction coefficient can be easily obtained. By using the relationship between the maximum friction coefficient and the maximum acceleration of a car, Equation 4.3 can be derived.

$$\begin{aligned} |a_x|_{max} &= \max|\frac{F_{x11}+F_{x12}+F_{x21}+F_{x22}}{m}| = \max|\frac{\mu N_s}{m}| \\ &= \max|\frac{\mu mg}{m}| \leq \mu_{max} g \end{aligned} \tag{4.3}$$

In Equation 4.3, g is the gravitational constant, and m is the total mass of a vehicle. Therefore, the maximum acceleration of a vehicle, while it is in motion, can be determined by estimating μ_{max}. For ABS(Anti lock Brake System), TCS(Traction Control System)or VDC(Vehicle Dynamics Control system), it is not possible to increase the maximum acceleration limit even though such systems are operated when a driver needs acceleration or deceleration that exceeds μ_{max}.

However, a μ_{max} estimator provides in real time the information to a human or machine driver that can prevents emergency situation. Hence, not only does it provides improvement in safety, but also it increases the efficiency of Vehicle Distance Control System.

Figure 4.1 shows the well known relationship between the longitudinal slip ratio of a tire and friction coefficient(Normalized longitudinal force). When slip increases, normalized longitudinal force also increases; however, after reaching the maximum value, normalized longitudinal force gradually declines. As for the braking condition, when the brake pressure is increased and exceeds the certain pressure, the slip of a wheel excessively occurs and the longitudinal force gradually decreased. Therefore, this research will estimate the maximum friction coefficient on the basis of this relationship shown in Figure 4.1.

Slip on each wheel is the difference between the circumferential velocity of a wheel and translational velocity of a vehicle, and the definition of slip used in this research is shown in Equation (4).

$$s = \frac{r\omega - v}{\max(r\omega, v)} \tag{4.4}$$

v in Equation 4.4 is longitudinal velocity, ω is angular velocity of a wheel, and r is the tire effective radius. In order to obtain the relationship between

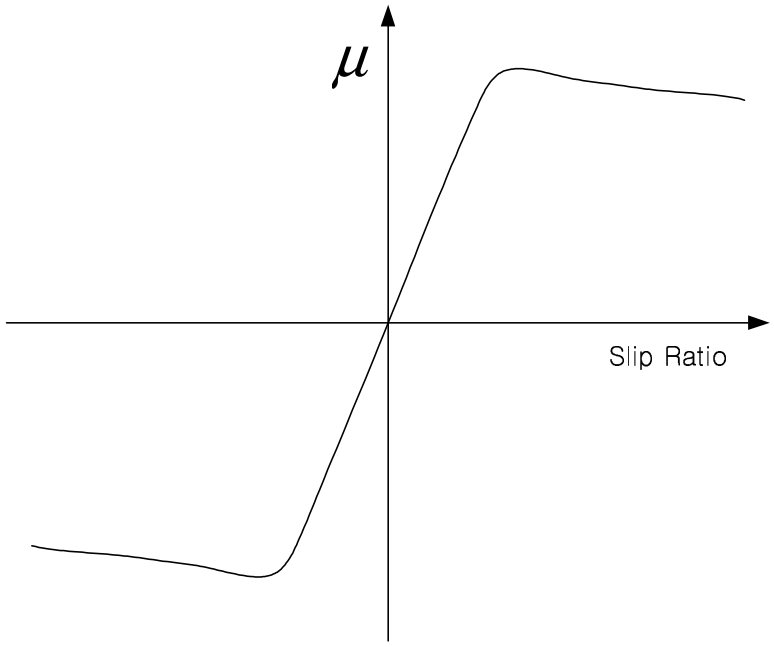

Figure 4.1: Longitudinal Slip Ratio Vs. Friction Coefficient.

slip and friction coefficient, Normal Force Estimator, Tire Effective Radius Estimator, Road Force Estimator are used. Also, a speed sensor is attached to each wheel, and the Fifth Wheel, which has almost zero slip, is attached to the rear bumper of the vehicle to measure the velocity.

4.2 Vehicle Speed and Wheel Speed Detection

On each wheel, Magnetic Pulse Detector is attached, and the angular velocity of a wheel can be measured with the series of magnetic pulse. However, the magnetic pulse contains lots of noise, and Kalman Filter is used to filter noise.

$$\begin{bmatrix} \dot{x_1} \\ \dot{x_2} \end{bmatrix} = \begin{bmatrix} 0 & 1 \\ 0 & 0 \end{bmatrix} \begin{bmatrix} x_1 \\ x_2 \end{bmatrix} + \begin{bmatrix} 0 \\ 1 \end{bmatrix} \omega \tag{4.5}$$

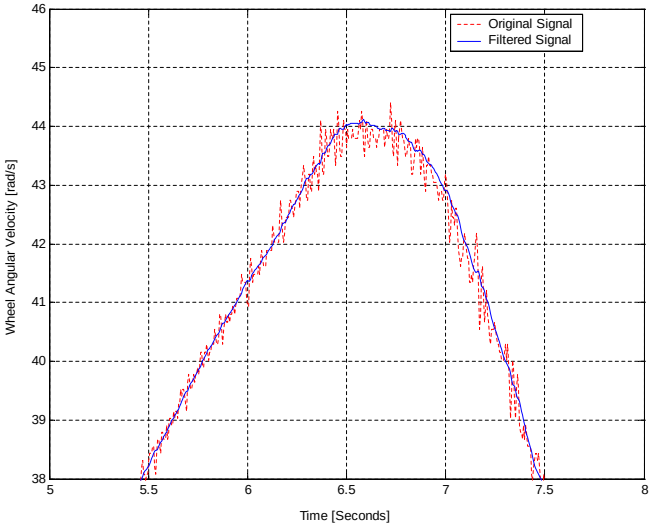

Figure 4.2: Wheel Angular Velocity Signal

$$y = \begin{bmatrix} 1 & 0 \end{bmatrix} \begin{bmatrix} x_1 \\ x_2 \end{bmatrix} + v \tag{4.6}$$

x_1, x_2 are angular velocity and angular acceleration of a wheel, and ω, v represents system disturbance and sensor noise, respectively.

$$\dot{\hat{x}} = A\hat{x} + L(y - \hat{y}) = (A - LC)\hat{x} + Ly \tag{4.7}$$

$$\dot{\hat{x}} = \begin{bmatrix} L_1(x_1 - \hat{x}_1) + \hat{x}_2 \\ L_2(x_1 - \hat{x}_1) \end{bmatrix} \tag{4.8}$$

L_1 and L_2 are Kalman filter gain.

Figure 4.2 shows the comparison between the original signal and the filtered signal.

Using Magnetic Detector the number of teeth on Fifth Wheel over a certain amount of time is measured. With the result and through the magnetic signal process shown in Figure 4.4, the velocity of the vehicle can be measured.

Figure 4.5 shows the actual velocity and filtered velocity, which uses Low Pass Filter.

Figure 4.3: Fifth Wheel

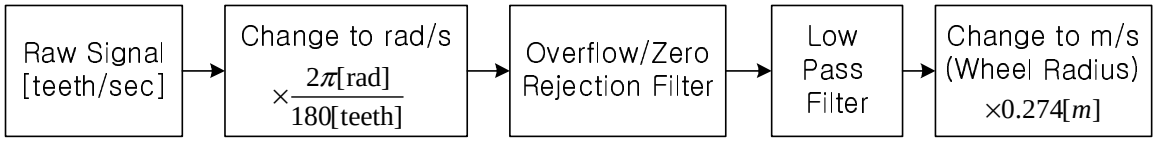

Figure 4.4: Velocity Detection Procedure

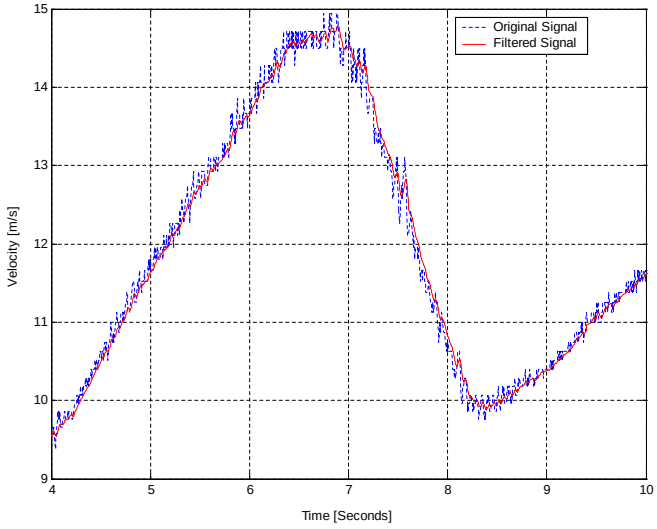

Figure 4.5: Velocity Signal Filtering using Low Pass Filter

4.3 Normal Force Estimator

To obtain the friction coefficient between road and a tire, normal force applied on each wheel needs to be calculated. Also, the exact circumference of each tire is needed to measure the exact slip. The circumference of each tire is exceptionally important to be measured because it is influenced by normal force a lot. Two ways are used to observe normal force on each tire: "Static Normal Force Estimator" which analyzes the vehicle statically and "Dynamic Normal Force Estimator" which considers both suspension and pitch motion. Figure 4.6 shows the model for Static Normal Force Estimator, and normal forces applied on front and rear wheels are represented in Equation 4.9. Figure 4.7 shows Dynamic Normal Force Model which includes suspension and tires. Using dynamic equations, normal forces applied on all four wheels are shown in Equation 4.10.

$$N_f = \frac{mgl_r - mah}{l_f + l_r}, \quad N_r = mg - N_f \tag{4.9}$$

$$\begin{aligned} F_{nf} &= 2k_{tf}R_u - (h_f + z_{uf}) \\ F_{nr} &= 2k_{tf}R_u - (h_r + z_{ur}) \end{aligned} \tag{4.10}$$

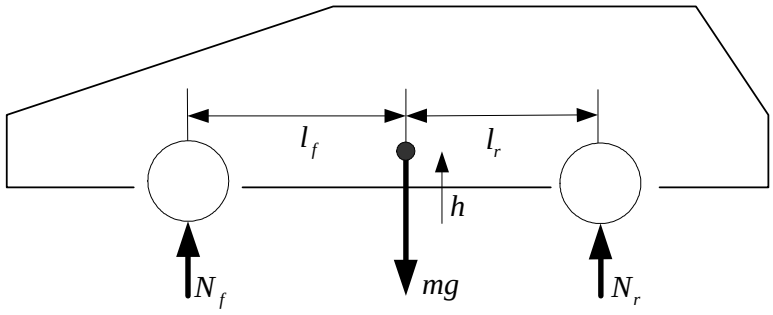

Figure 4.6: Static Normal Force Model

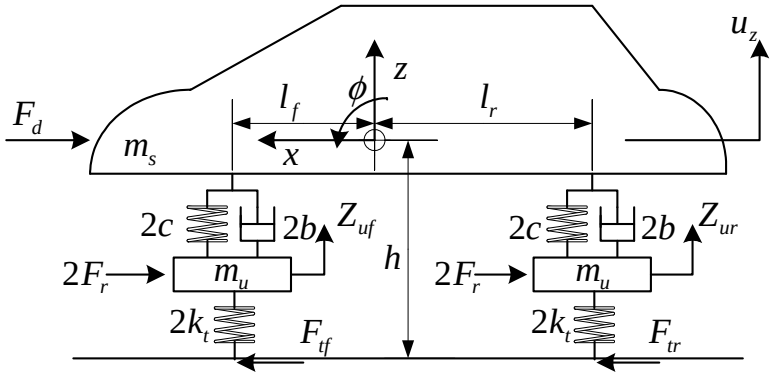

Figure 4.7: Dynamic Normal Force Model

Figure 4.9 and 4.10 shows the normal force applied on wheels using static/dynamic normal force estimator supposing the vehicle has the same velocity profile shown in Figure 4.8. As shown in Figure 4.9 and 4.10, static normal force and dynamic normal force have a similar value. Hence, in an attempt to lessen the calculation load of the system, the static normal force estimator is used.

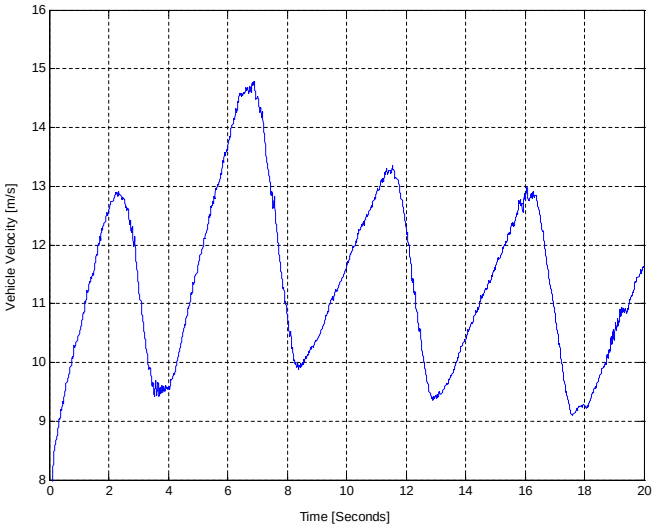

Figure 4.8: Velocity Profile for Normal Force Estimator

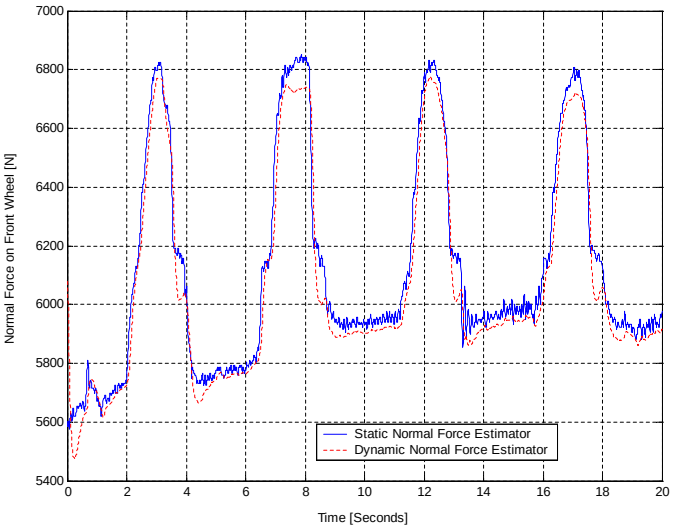

Figure 4.9: Normal Force on Front Wheel

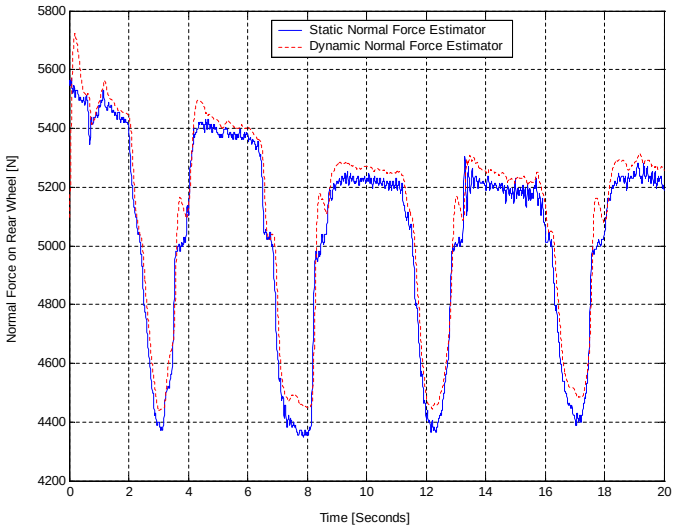

Figure 4.10: Normal Force on Rear Wheel

4.4 Tire Effective Radius Estimator

If the slip ratio is less than 0.05 in normal driving situation, it is very important to know the range of valid tire circumference. Specially, the tire circumference constantly changes depending on air pressure of the tire, speed, and normal force. Figure 4.11 shows the spring constant of the tire depending on the air pressure of the tire. Also, as shown in Figure 4.12, as the vehicle velocity increases, the circumferences of all four tires increase with the slope of 0.0004 [m/(m/s)].

Therefore, when normal force, vehicle speed, and tire pressure are considered, the amount of change in circumference of a tire can be shown in Equation 4.11.

$$\Delta R = \frac{F_{No} - k_v k_t v}{k_t F_{No}} \times F_N \tag{4.11}$$

Here, F_{No} is the initial normal force when the vehicle stops, and $F_N$is the actual normal force when the vehicle is in motion, and it is obtained from Normal Force Estimator. k_v is the velocity constant of tire (0.0004 [m/(m/s)]), k_t is the tire spring constant, and v is the velocity of the vehicle. However, the actual circumference when the vehicle is in motion is shown in

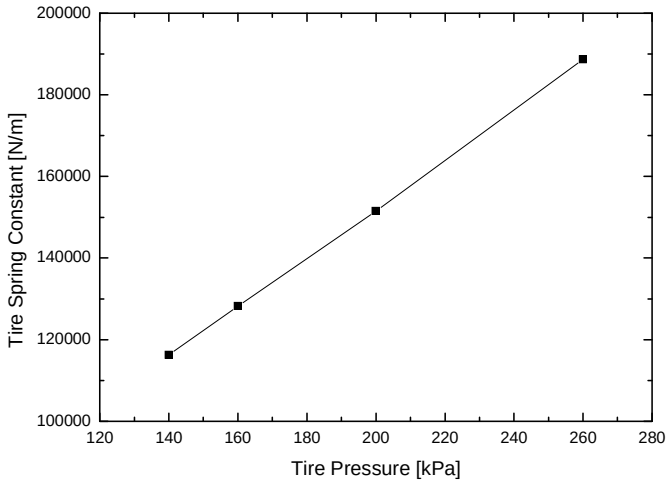

Figure 4.11: Tire Spring Constant Change with Tire Pressure

Equation 4.12.

$$R_e = R - \frac{1}{k_r}\Delta R \tag{4.12}$$

Here, k_r is constant value depending on tire and usually is the value of 3. Figure 4.13 shows the estimation of tire radius using Equation 4.11 and 4.12 under free rolling situation. and Figure 4.14 shows the effective radius estimation using the velocity profile of Figure 4.8

4.5 Road Force Estimation

With ordinary automotive sensor, road force applied to a tire cannot be observed. However, in this research a strain gauge is attached between the front left brake disk and the wheel to obtain brake torque, which occurs when braking. The dynamic equation of a wheel is shown as in Equation 4.13, and the road force applied on tire can be determined as in Equation 4.14.

$$J\dot{\omega} = -T_B - F_t r \tag{4.13}$$

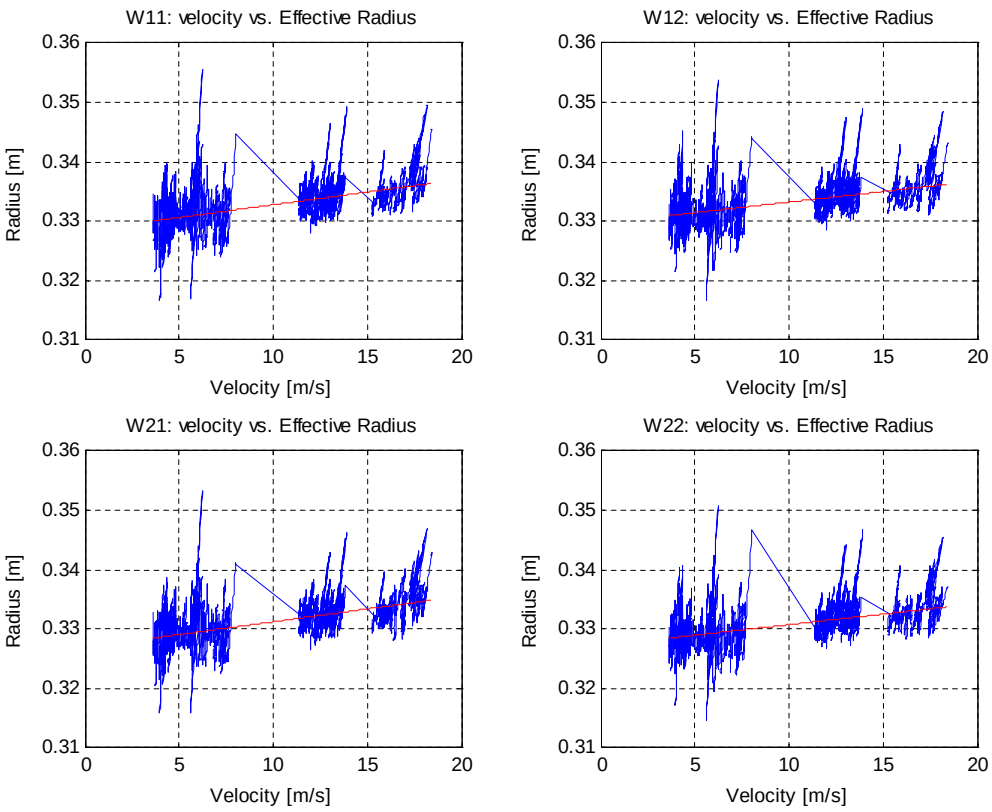

Figure 4.12: Tire Radius vs. Vehicle Speed

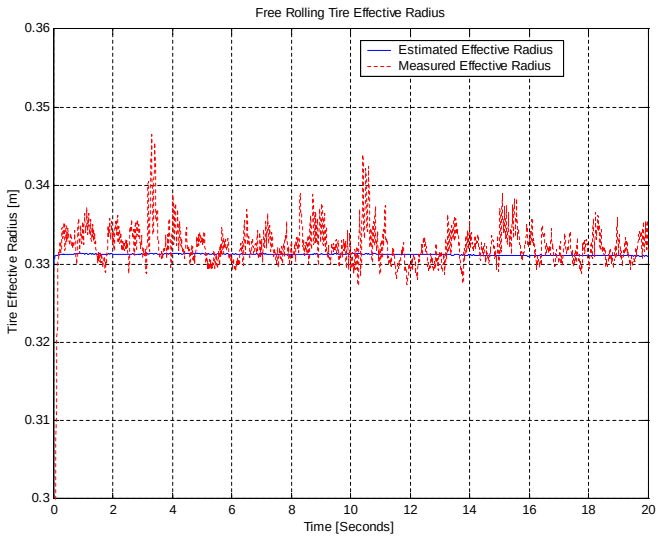

Figure 4.13: Effective Tire Radius Estimator under Free Rolling

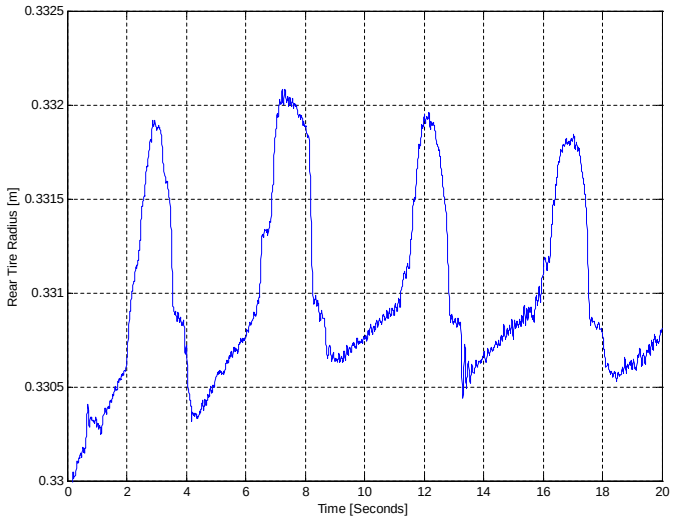

Figure 4.14: Effective Tire Radius Estimation

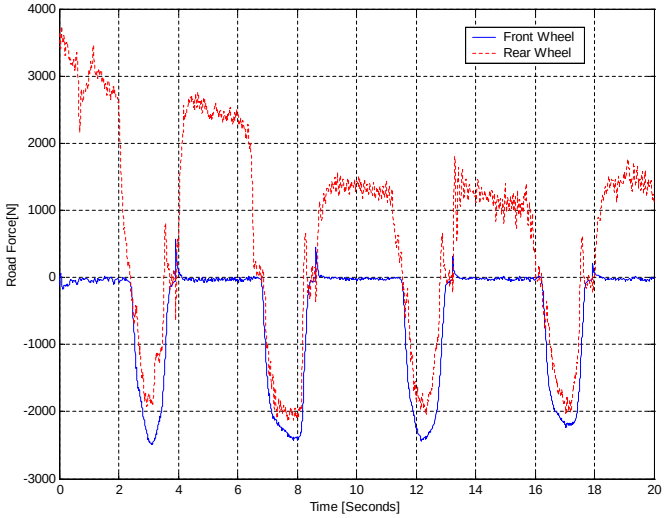

Figure 4.15: Road Force Estimation

$$F_t = \frac{(-T_B - J\dot{\omega})}{r} \tag{4.14}$$

Therefore, supposing the brake torques on front left wheel is same with that of front right wheel, the road force applied on front right wheel can be determined. Also, as vehicle dynamics equation is equivalent to Equation 4.16, road force applied on rear wheels can be found in Equation 4.16.

$$m\ddot{u_x} = -F_d - F_r + (F_{t11} + F_{t12} + F_{t21} + F_{t22}) \tag{4.15}$$

$$F_{t21} + F_{t22} = m\ddot{u_x} + F_d + F_r - (F_{t11} + F_{t12}) \tag{4.16}$$

Here, F_d, F_r represents drag force and rolling resistance, respectively. Figure 4.15 shows the road force estimation when the vehicle has the same velocity profile as in Figure 4.8.

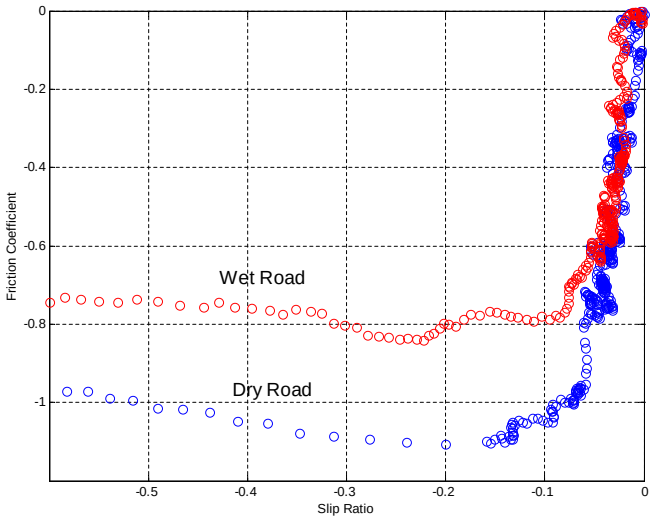

Figure 4.16: Slip Curve under different road condition

4.6 Slip Slope Detection for Maximum Friction Coefficient Estimation

It is widely known that depending on the road condition, the slope and even the maximum friction coefficient in slip vs. friction coefficient graph change. Therefore, under a certain value of slip, the slope is different depending on the characteristic of the road condition: dry, wet, snowy and icy. In this research, using the special behavior of slip that occurs when the brake pressure is linearly increased on dry and wet asphalt road, the full slip curve can be obtained as shown in Figure 4.16. In order to monitor the road condition using initially low slip, the slip within the range of -0.02 0.02 is used. As shown in Figure 4.17, slips on dry asphalt road and wet asphalt road are definitely different. Slip and friction coefficient have a linear relationship as shown in Equation 4.17, and using the linear regression method the slope can be found.

$$\mu = k \cdot s \tag{4.17}$$

Also, to monitor the road condition in real time, Recursive Least Square Estimation with the Forgetting Factor is used.

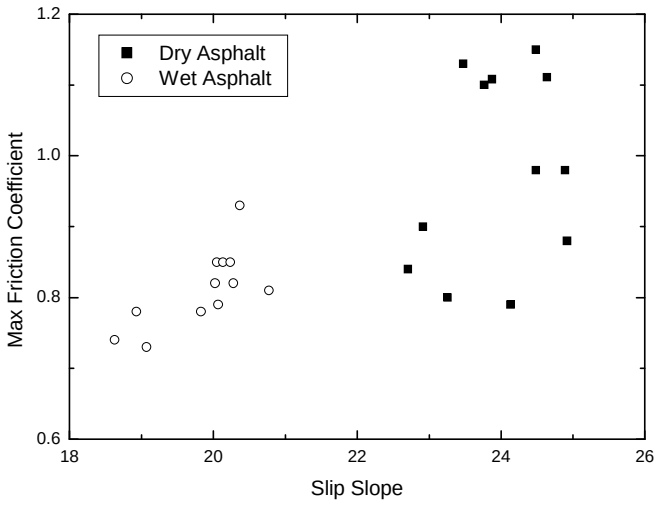

Figure 4.17: Maximum Friction Coefficients Distribution

$$y(k) = \theta\phi(k)^T \tag{4.18}$$

$$\hat{\theta}(k+1) = \hat{\theta}(k) + \frac{F(k)\phi(k) - \hat{\theta}(k)^T\phi(k)}{\lambda + \phi(k)^T F(k)\phi(k)} \tag{4.19}$$

$$F(k+1) = \frac{1}{\lambda}\left[F(k) - \frac{F(k)\phi^T(k)\phi(k)F(k)}{\lambda + \phi^T(k)F(k)\phi(k)}\right] \tag{4.20}$$

Here in these equations, F and λ are adaptive gain and forgetting factor, respectively. Using this method, Figure 4.18 and 4.19 express slip slope with varying forgetting factor when acceleration and deceleration repeatedly occur on dry and wet road.

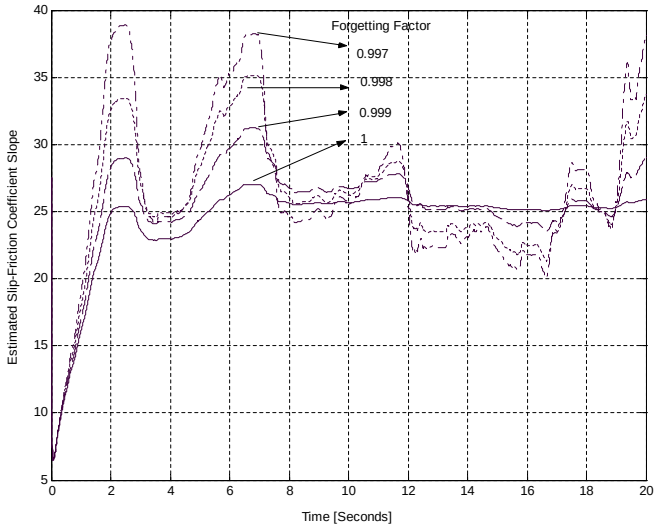

Figure 4.18: Slip Slope Estimation using Recursive Least Squares [Dry Road]

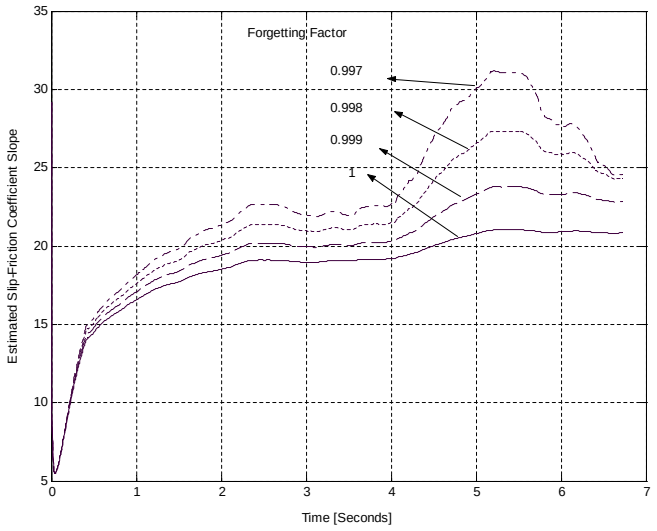

Figure 4.19: Slip Slope Estimation using Recursive Least Squares [Wet Road]

Chapter 5

Emergency Braking Maneuvers of Single Vehicle

5.1 Introduction

Traditionally the control strategy in an emergency situation has been to bring a vehicle to a stop as quickly as possible. This is the motivation behind such concepts as anti-lock brake systems(ABS). However, in an Automated Highway System, traffic is organized into platoons with relatively small distances. The platoon must ensure that the vehicles will not collide each other even if the platoon ahead of it brakes abruptly. There have been several research efforts in PATH dealing with emergency braking of the platoon. Alvarez and Horowitz used a collision-free notion of safety to design de-coupled platoon maneuvers in the case when platoons have different braking capabilities in [7]. Under MOU 319, the vehicle motion and collision is modelled as a hybrid system and the safety conditions under certain deceleration strategies are suggested [21] [31]. In this project, a slip-based brake controller capable of performing under high-slip conditions is proposed which will reduce the tracking errors induced by the the excessive force.

Nonlinear sliding mode control has proven effective in addressing the nonlinearities and parametric uncertainties associated with vehicle control. This strategy has been working very well under normal driving conditions. However, the problem with this approach, and vehicle control in general, is that the control inputs of the engine and brake torque enter in at the wheel, while it is ultimately desired to control the motion of the vehicle as a whole. In

order to relate the desired vehicle dynamics to desired wheel dynamics, a limited slip assumption is applied. This is based on the familiar kinematic relationship between linear(v) and angular velocity(ω) under rolling without slip:

$$v = r\omega \tag{5.1}$$

While under normal driving this assumption is reasonable, it does not hold under hard braking or acceleration. In order to overcome this limitation, a brake controller that uses the empirical relationship between road force and wheel slip to relate the wheel dynamics to the vehicle dynamics has been suggested and evaluated. Theoretically, a new controller can compensate for the errors accumulated from the limited slip assumption and improve the braking performance. In this chapter, a controller with a limited slip assumption and a slip-based controller are introduced. Then, the simulation results of the two controllers are presented. Also, the experiments of an emergency braking maneuver are executed and the characteristic behaviors of a vehicle under emergency braking are analyzed.

5.2 Control Methods for the Emergency Braking

In this project, a new control method based on the idea of using tire slip data for the precise control of the vehicle longitudinal motion is developed. Typical behavior of an emergency braking maneuver can be characterized by a rapid deceleration which will induce a large amount of slip in the tire. In such a situation, the limited slip assumption on which previous nonlinear longitudinal vehicle control is based is not valid. We will analyze the performance and availability of a new slip-based controller and compare it with those of nonlinear control methods based on the limited slip assumption.

5.2.1 Controller with Limited Slip Assumption

In this section, a simplified model of the vehicle dynamics for control purposes is described. It is assumed that the torque converter is locked, therefore the dynamics of the torque converter are neglected.

In the vehicle system there are two levels of dynamics that we are concerned with. One level is the dynamics of the vehicle as a whole, and the

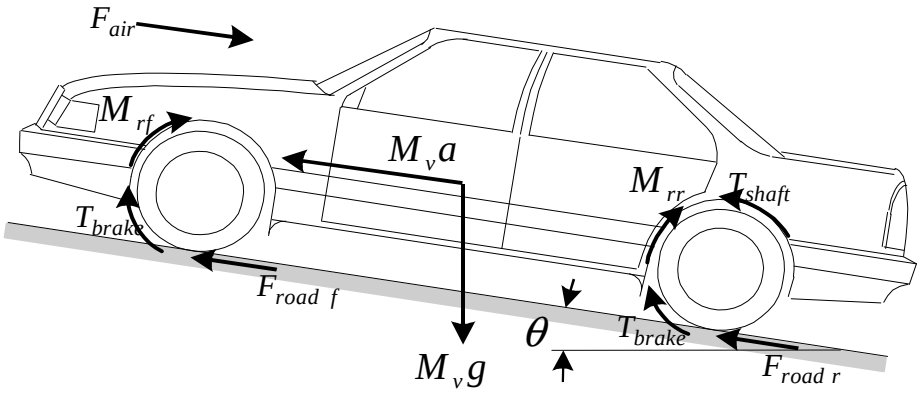

Figure 5.1: Vehicle System Dynamics.

other is the dynamics of the wheels. The dynamics are represented by

$$M_v \dot{v} = F_{road} - F_{roll} - F_{air} - \Delta f_1 \tag{5.2}$$

$$J_w \dot{\omega} = T_{shaft} - T_{brake} - hF_{road} - \Delta f_2. \tag{5.3}$$

M_v represents the mass of the vehicle, J_w the rotational inertia of the wheel, and h denotes the effective radius of the wheel. Δf_1 and Δf_2 denote the modelling uncertainty. Road grade is omitted in the analysis for simplicity.

In practice, aerodynamic drag force (F_{air})is usually expressed in the following form:

$$F_{air} = C_d v^2 \tag{5.4}$$

which is proportional to the square of vehicle speed.

The rolling resistance(F_{roll}) of the tire is primarily caused by the hysteresis in tire materials due to the deflection of the carcass while rolling. Based on experimental results many empirical formulas have been proposed for calculating the rolling resistance of the tires. In this project, aerodynamic friction is ignored, and the rolling resistance is assumed to be constant over the entire operating region.

Table 5.1 summarizes the vehicle parameters used for all the simulations. These parameters were obtained from those of the experimental vehicle used by PATH, and this vehicle is used to experimentally verify the suggested control algorithm.

Mass (M_v)	2000 Kg
Wheel moment of inertia (J_w)	1.93 Kg/m^2
Aerodynamic drag coefficient (C_d)	0.53
Wheel effective radius (h)	0.33 m
Rolling resistance (F_{roll})	172 N
Engine inertia (J_e)	0.2630 Kg/m^2
Gear ratio	[0.4167, 0.6817, 1.0, 1.4993]
Final drive ratio	0.3058

Table 5.1: Vehicle Parameters

To control the longitudinal motion of the vehicle, a nonlinear control method called 'Dynamic Surface Control' is used. Dynamic surface control is a method which avoids the explosion of terms when designing a multiple sliding surface controller. Also this controller holds the robustness property which is one of the typical characteristics of most nonlinear controllers. We assume the vehicle dynamics and wheel dynamics described in equation 5.2 and 5.3, are related by

$$v = h\omega. \tag{5.5}$$

Then, we have the following combined equation.

$$\dot{v} = \frac{1}{\beta}\{T_{net} - h(F_{air} + F_{roll} + \Delta f_1) - \Delta f_2\} \tag{5.6}$$

where T_{net} and β are represented by

$$T_{net} = (\frac{T_e}{R_g} - T_b) \tag{5.7}$$

and

$$\beta = (M_v h + \frac{4J_w}{h} + \frac{J_e}{hR_g^2}) \tag{5.8}$$

where J_e denotes the engine inertia. R_g represents the combined coefficient of gear ratio and final drive ratio so that equation 5.9 holds.

$$\omega_e = \frac{\omega}{R_g}. \tag{5.9}$$

The control objective of the longitudinal vehicle motion is tracking a desired velocity profile while maintaining a desired level of spacing with the

vehicle it is following. To describe this control goal, a sliding surface S is defined in terms of the spacing error(ϵ) between the preceding and following vehicle.

$$S = \dot{\epsilon} + \lambda\epsilon. \tag{5.10}$$

Taking the derivative of our surface S_1, we get

$$\dot{S} = \ddot{\epsilon} + \lambda\dot{\epsilon} = (a_{des} - a) + \lambda(v_{des} - v). \tag{5.11}$$

If the control input is defined so that it tries to push the defined surface S to zero, then according to this equation 5.11, ϵ will also asymptotically converge to zero. This can be accomplished if we choose the control input to make the Lyapunov function defined below, satisfy the stability condition.

$$V = \frac{1}{2}S^2 \tag{5.12}$$

This quadratic form of the Lyapunov function is positive definite, and if our control input makes $\dot{S} = -\eta S$, then $\dot{V} = -\eta S^2$ is negative definite, therefore our Lyapunov function satisfies the asymptotic stability conditions.

Assuming a linear relation between brake pressure and brake torque of $T_b = K_b P_w$ the control input satisfying those stability conditions are as follows.

$$P_{w\,des} = \frac{1}{K_b}\Big[\frac{T_e}{R_g} - h(F_{air} + F_{roll} + \Delta f_1) - \Delta f_2 - \beta\{a_{des} - \lambda(v - v_{des}) + \eta S\}\Big] \tag{5.13}$$

If we have the control gain η large enough to overcome the model uncertainty, then the above control law will have the desired robustness property, but a large control gain is not desired from the optimal point of view. In practical applications, it is difficult to know how much uncertainty we have, so the control gain is tuned by trial and error.

5.2.2 Slip-based Controller

In the control algorithm suggested above, the wheel dynamics and vehicle dynamics are combined into one equation using the assumption that vehicle speed is the multiplication of wheel effective radius and wheel rotational speed. This assumption is valid as long as we have small traction forces

acting on the tire. However, as the vehicle accelerates or decelerates, the gap between vehicle speed and the multiplication of wheel radius and rotational speed increases because of the heavier traction force. Hence, to quantify those differences, slip is defined as equation 5.14.

$$s = \frac{r\omega - V}{max(r\omega, V)} \tag{5.14}$$

When driving torque is applied, the tire rotates without the equivalent translatory progression, therefore, $r\omega > V$ and a positive value for slip results. When braking torque is applied instead, $r\omega < V$ and a negative value for slip results. Many theories deal with this relationship between the road force and tire slip, and the Bakker-Pacejka 'Magic Tire Formula' of the form in equation 5.15 is employed in this study.

$$s = D\sin(C\arctan[B(s+S_h) - E(B(s+S_h) - \arctan(B(s+S_h)))]) \tag{5.15}$$

The fundamental idea behind the design of a slip-based controller is that we can use the above empirical relationship between road force and slip. Then, we don't need to combine the vehicle and wheel dynamics, assuming that the vehicle speed and the multiplication of wheel radius and rotational speed are the same. Each dynamic equation can be solved by applying the tractive force calculated from the above magic tire formula to get a more precise control law suitable for an emergency braking maneuver.

The first step in the design of this controller is to define the sliding surface. The first surface dealing with space tracking is identical with the previous control method described in equation 5.10. But instead of using the combined equation of vehicle and wheel dynamics, vehicle dynamics equation 5.2 is substituted into equation 5.11 to get the following equation.

$$\dot{S}_1 = a_{des} - \frac{1}{M}(F_{road} - F_{air} - F_{roll} - \Delta f_1) + \lambda(v_{des} - v) \tag{5.16}$$

Choosing a synthetic input(v_1) as F_{road}, the synthetic input should have the following value to make the first surface stable.

$$v_1 = M\{a_{des} + \lambda(v_{des} - v) + \eta_1 S_1\} + F_{air} + F_{roll} + \Delta f_1 \tag{5.17}$$

The second surface is defined as,

$$S_2 = v_1 - v_{1\,des}. \tag{5.18}$$

For this second surface we don't want to take the derivative of the desired road force because that information is unknown, therefore the technique of the dynamic surface control is employed. The filtered value is defined in equation 5.19.

$$\tau_2 \dot{v}_{1\,des\,filt} + v_{1\,des\,filt} = v_{1\,des} \tag{5.19}$$

By choosing tau_2 sufficiently small, the lag due to the filter will be minimized, and this approximation becomes reasonable.

Then the derivative of the first surface is described as,

$$\dot{S}_2 = \dot{v}_1 - \dot{v}_{1\,des} \approx \dot{F}_{road} - \dot{v}_{1\,des\,filt}. \tag{5.20}$$

Next, taking the derivative of the road force at each wheel makes the wheel dynamics appear.

$$\dot{F}_{road} = \sum \frac{\partial f_i}{\partial s_i} \dot{s}_i = \sum \frac{\partial f_i}{\partial s_i} (\frac{r_i \dot{\omega}_i}{V} - \frac{r_i \omega_i \dot{V}}{V^2}) \tag{5.21}$$

Substituting the wheel dynamics and the vehicle dynamics from equation 5.3 and 5.2, one can see that our control input, master cylinder pressure, now has access to our states through the brake pressure at the wheel. The final control input on the master cylinder pressure is expressed in equation 5.22,

$$\begin{aligned} P_w \;=\; & \{\sum \frac{\partial f_i}{\partial s_i} \frac{h_i b_i K_b}{J_w + a_i \frac{J_e}{R_g^2}}\}^{-1} \Big[\sum \frac{\partial f_i}{\partial s_i} \frac{h_i (h_i a_i T_e - h_i f_i - \Delta f_2)}{J_w + a_i \frac{J_e}{R_g^2}} \\ & - \sum \frac{\partial f_i}{\partial s_i} \frac{h_i w_i}{M_v v} (\sum f_i - F_{air} - F_{roll} - \Delta f_1) - v(\frac{v_{1\,des} - v_{1\,des\,filt}}{\tau_2} \\ & - \eta_2 S_2) \Big] \end{aligned} \tag{5.22}$$

where a_i and b_i represents the ratio of shaft and brake torque distributed to each wheel, and $\sum$ denotes the summation over all four wheels.

5.2.3 Simulation Results

The desired velocity profile command to the controller is shown in figure 5.2, where the deceleration is set to be $-7m/s^2$. This deceleration is almost the maximum rate of velocity which our experimental vehicle can follow without locking its wheels. It is assumed that in an emergency situation, vehicles in

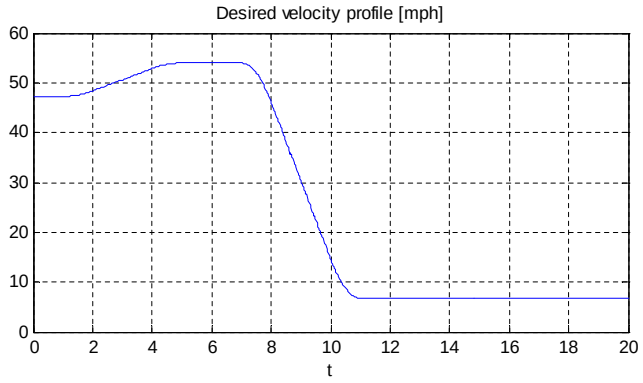

Figure 5.2: Desired Velocity Profile.

the platoon will try to follow a certain desired velocity profile decelerating as fast as they can. Also the designed controllers are assumed to have the exact modelling parameters of the vehicle. However, even with some modelling or parameter uncertainties, both nonlinear controllers showed nice robustness properties in the simulation result.

In an automated highway system the inter-vehicle spacing is expected to be very small to increase the road capacity of the traffic. Therefore, space tracking errors should be minimized for the vehicles in a platoon to avoid collision during emergency braking. Figure 5.3 (a) and (b) shows the space tracking error of the two controllers during the simulation. It is observed that the maximum space tracking error of the slip-based control is smaller than that of the limited slip controller. According to this results, the vehicles controlled by the developed slip-based controller is expected to have a smaller chance of collision during the emergency braking maneuver.

Figure 5.3 (c) and (d) shows the slip generated on the tire during the simulation. Excluding the peak values of impulsive slip change, the maximum slip occurs around 0.04 which is quite large with the tire model we used. This is because the maximum friction coefficient of the experimental vehicle is found near the slip of 0.05 in normal driving condition.

We can conclude that the slip-based controller reduced the tracking error and improved the control performance slightly. However, the simulation results do not show a significant performance improvement. This is because our simulation is limited to the -0.05–0.05 slip range, and this is not an enough slip to break the limited slip assumption. The concept of slip-based control is proposed because of the significant amount of slip that will be generated

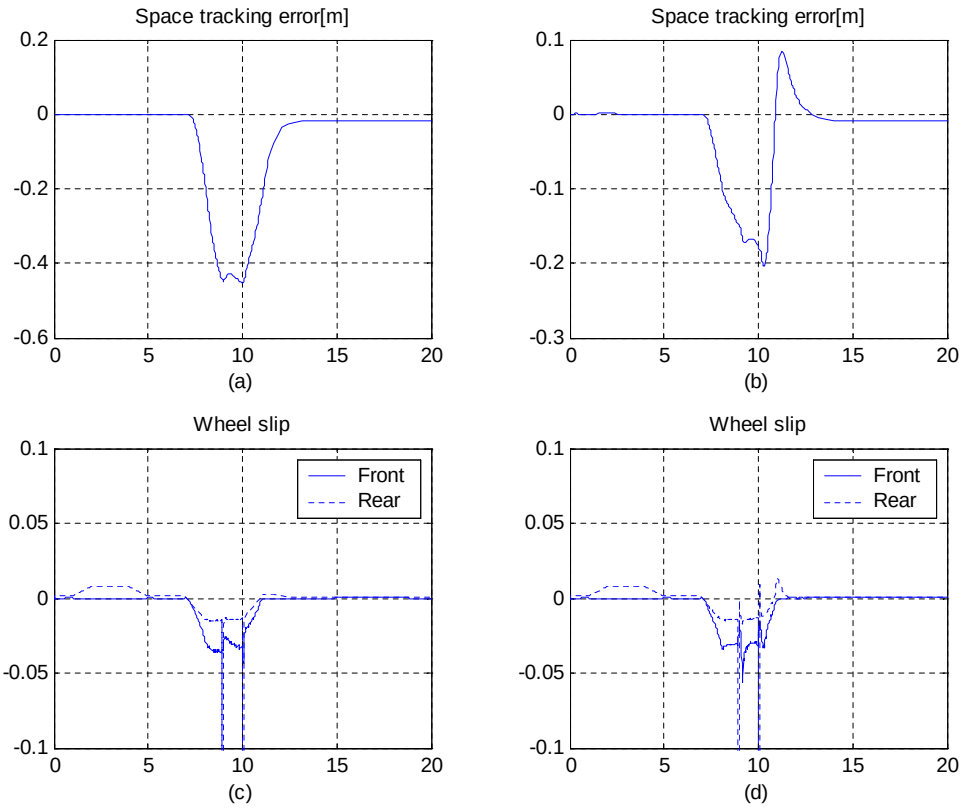

Figure 5.3: (Using stiff tire model)(a) Space tracking error of the controller assuming limited slip. (b) Space tracking error of the slip-based controller. (c) Slip on each wheel with the controller assuming limited slip. (d) Slip on each wheel with the slip-based controller.

during an emergency braking situation. However, as long as vehicles are equipped with anti-lock braking systems, the slip will not go beyond the value of the maximum friction coefficient, hence the limited slip assumption is still valid. Besides the limitation on slip due to the anti-lock brake systems, it is undesirable for the vehicle to have a large amount of slip because the excessive slip will make the wheels lock and cause the vehicle to be unstable and lose maneuverability. Using the slip data for control will not be worth the expense of the complex calculation and the risk of introducing slip measurement noise as long as the controller limited slip assumption holds and the controller is robust enough to handle the errors caused by the assumption. From the above simulation results, it is assured that the existing controller has enough performance even in an emergency braking situation and in the next chapter it will be verified experimentally.

5.3 Experimental Testing of Emergency Braking

Vehicles equipped with the necessary sensors and actuators are used to experimentally verify the performance of the controller designed in this project. Simulations provided a qualitative understanding of controller performance. However, performance in a real world environment still has to be assessed.

The simulation results of section 5.2 showed that the both of the controllers will track the desired longitudinal motion without causing too much tracking error during emergency braking. Hence, we made an experiment with the controller assuming limited slip only, and the performance of the controller in a real situation is checked.

The emergency maneuver of the vehicle on the dry and wet surface is tested and the problems of applying current control strategy to the emergency braking is analyzed.

5.3.1 Experimental Setup

All of the experimental work was performed on the Red Lincoln Towncar provided by California PATH. The actuators on the vehicle consist of a stepper motor on the throttle valve, and pump accumulator system that generates hydraulic pressure to actuate the vehicle's master cylinder. It should be

noted that the brake actuator has been characterized as having a 30 msec pure time delay, as well as a first order lag of 20 msec.

Wheel rotational speed sensors implemented on the experimental vehicle output two signals: one optimized for low speed and the other for high speed. Vehicle velocity is measured by the extra 5th wheel contacting the road surface and rolling freely with constant radius. By counting the teeth of gears on the wheel for a constant period, vehicle velocity can be estimated. Brake pressure sensor at the wheel and master cylinder is determined from pressure transducers.

The control code for this vehicle is implemented in C on a Pentium processor running the QNX operating system. The C code for the QNX computer is automatically generated using the Real-Time Workshop toolbox of MATLAB from a Simulink file composed of data input and output ports, data processing blocks, and controller blocks. This procedure enables us to directly implement the controller used in the simulation to the experimental vehicle.

5.3.2 Controller Performance

The experiment was performed on the track in Richmond Field Station, and the desired velocity profile commanded to the controller is shown in figure 5.4. The vehicle could not be driven as fast as it is in the simulation due to the speed limit on the test track, so the deceleration was maintained only for a short period.

For the first 7 seconds, the vehicle is commanded to maintain a constant speed because we want each result to have the same initial condition before braking so that the clear effect of the emergency braking can be shown. Then, the vehicle is commanded to decelerate as fast as -8 m/s^2 until it stops. The same test was performed on the dry surface and wet surface to observe the effect of the different friction coefficient on the control performance.

In figure 5.5 (a) the space tracking errors on the dry and wet surface are plotted. Similar to the simulation results, the errors increase as the deceleration proceeds. However, due to the modelling or parameter uncertainty, more errors are measured than were shown in the simulation results.

Negative space tracking errors imply that the inter-vehicle distance has been reduced and as long as the maximum errors are lower than the inter-vehicle spacing, a collision will not occur.

In the figure 5.5 (b) the gap between the actual velocity and desired

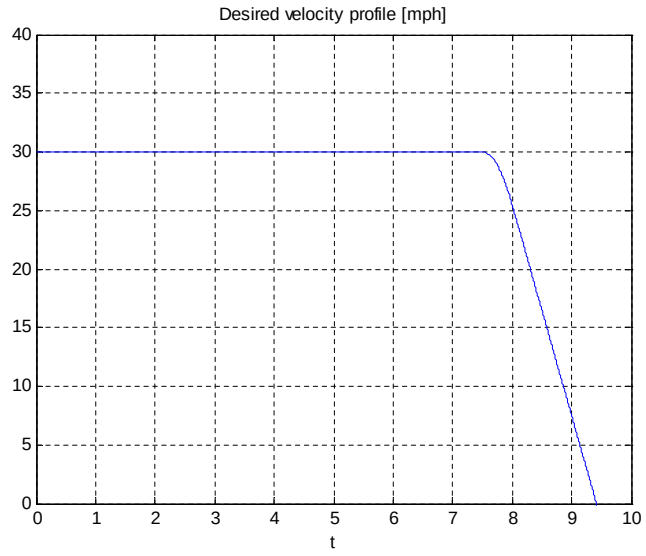

Figure 5.4: Velocity Profile of the Experimental Vehicle

velocity is larger on the wet road than on the dry road because of the limited availability of the friction force on the wet road.

5.3.3 Emergency Braking Vehicle Behavior

In figure 5.6, the wheel speed and the slip generated during the test is plotted. It is observed that as the errors increase during the braking, more control efforts are applied to compensate for the errors, and the slip increases as error to make the wheels lock. These results are not observed on the dry road, but obvious on the wet road. In figure 5.6 (b) and (d), the front wheels almost lock making the slip as small as -0.5.

If the controller eventually makes the wheels lock when the friction coefficients are low, it may not be a good control strategy for an emergency braking situation. The maximum friction coefficient estimation technique will help to avoid such a situation. Also the cooperative control strategies can be beneficial to avoid rear-end collision of the platoon.

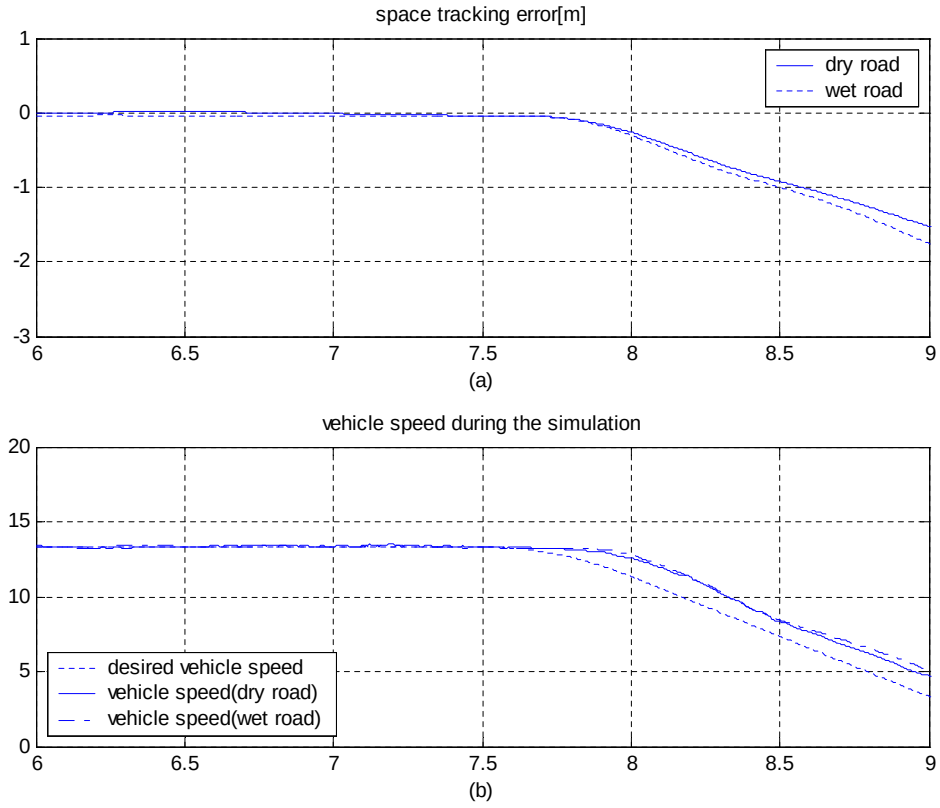

Figure 5.5: (a) Space tracking error on the dry and wet road (b) Velocity profile on the dry and wet road

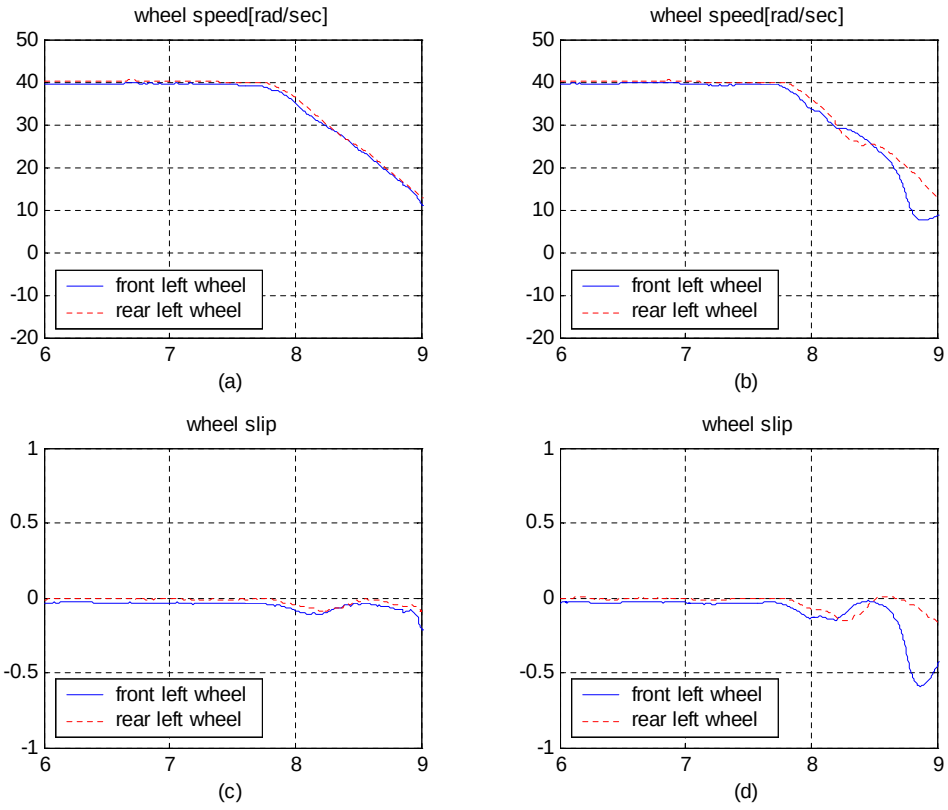

Figure 5.6: (a) Wheel speed on the dry surface (b) Wheel speed on the wet surface (c) Wheel slip on the dry surface (d) Wheel slip on the wet surface

Chapter 6

Emergency Braking Control using String Stable Controller

6.1 Introduction

The safety in an emergency braking situation is the most critical factor in an automated highway system (AHS). In the architecture of an automated highway system, California PATH (Partners for Advanced Transit and Highways) has been using the concept of platoons in which traffic is organized in groups of closely spaced vehicles. In this paper, a safe control strategy is considered in the situation when the platoon needs to decelerate rapidly. The goal is to design a control strategy such that rear end collisions can be avoided taking into consideration the different braking abilities of each vehicle. Rear end collisions can occur when the controller commands deceleration greater than the vehicle's maximum limit. Therefore, in case of braking, a vehicle may skid its wheel and lose control. In general, the maximum deceleration limit of a vehicle is determined by its maximum friction coefficient between the road and tire as follows [18].

$$\|a\|_{max} \leq \mu_{max} g \tag{6.1}$$

where $\|a\|_{max}$ denotes the maximum deceleration limit, μ_{max} denotes the maximum friction coefficient between the road and tire, and g denotes the gravity constant.

Modern Antilock Brake Systems (ABS) are designed to avoid wheel-locking and the resulting unstable condition, even if the driver's braking

input is greater than the vehicle's maximum limit. However, if the maximum deceleration limit of each vehicle in a platoon is significantly different, the following vehicles with ABS will not decelerate at the same rate, and a collision may occur.

Previous studies concerning safety in the AHS is done by Grimm and Fenton [19] studying the key factors affecting accident severity in collisions and the required uniform headways. Li et all [30] studied the safe maneuvering region of platoons performing basic maneuvers such as join, split and change lane. Godbole and Lygeros [21] studied the results of emergency braking under constant headway policy and analyzed the safety and throughput in a large scale system. Swaroop and Hedrick [41], and Seiler et all [37], showed the benefits of using leader vehicle information to reduce error propagation in automated vehicle control.

In this paper, a proper regulation of reference trajectory given to the leading vehicle is studied using the string stable controller. In section 6.2, the assumptions made in this study are presented and the emergency situation of our interest is defined. Among several potential control strategies, the leader and the preceding vehicle following strategy is chosen and the properties of this strategy are explained in section 6.3 and 6.4. An illustrative example is given in section 6.5.

6.2 Control Strategies for the Platoon

In this section, several assumptions are made in order to simplify the platoon models in the AHS. Under those assumptions, control strategies that can enhance the safety in the defined emergency situation are considered. In this paper, we made the following assumptions.

1. The dynamics of the vehicles are considered to be identical except for the maximum acceleration and deceleration limits.

2. All the following vehicles use the same control law.

3. The desired inter-vehicle spaces are the same for each following vehicle.

4. Vehicles are equipped with sensors to measure the relative distance and velocity from the preceding vehicle, and also with a communication method to transmit the information to other vehicles.

5. The maximum acceleration and deceleration limit of each vehicle can be measured.

The fifth assumption means that we have the proper estimation technique such that the maximum friction coefficients between road and tire can be estimated and be transmitted to the leader vehicle or high level controller. Several friction estimation techniques have been suggested by many researchers. Some of them are cause-based, i.e. using optical sensors [9], and some are effect-based such as measuring the slip between the road and tire [34].

Among many situations that can be categorized into the emergency situations, we will consider the case when large deceleration of the whole platoon is needed. We will not consider the case when vehicles can change lanes to avoid the emergency situation. In such a situation, it is important that the controller does not command a larger input than its maximum deceleration limit, otherwise the vehicle will skid its wheels and lose control. In the AHS, where all the vehicles are forming a platoon with tight spacing, a single vehicle out of control can endanger the whole platoon. Therefore, it is important to know the maximum deceleration limit of each vehicle and regulate the control input properly to avoid dangerous situation.

The maximum deceleration limit of a vehicle is determined by the maximum friction coefficient between the road and tire. Ebert [16], shows that the standard deviation of the maximum friction coefficient for the same test surface can be as large as 0.05. In practice, they are supposed to vary more than that. Hence, emergency braking controller should be able to take into account differences of maximum deceleration limit.

The possible emergency braking strategies are as follows. First, there is a strategy in which all the vehicles in the platoon brake with their maximum deceleration limit when an emergency situation occurs. In this case, the difference of maximum deceleration limits and space between vehicles will determine whether the collision occurs or not.

Two other coordinated control strategies are preceding vehicle following, and the leader vehicle following strategy. Although the first propagates error and causes string instability, it is safer in the sense that each vehicle takes care of its own safety. Leader vehicle following does not propagate errors therefore ensures string stability, but can be dangerous when the previous vehicle does not keep good tracking of its given reference profile.

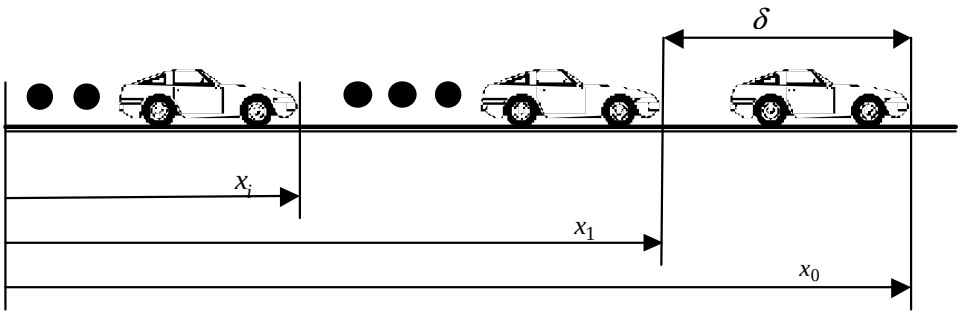

Figure 6.1: Vehicle System Dynamics.

By combining both control structures, we can take advantages of both control strategies and develop more robust control structure. In this paper, the term 'string stable controller' denotes the combination of both predecessor and leader vehicle following.

6.3 String Stable Controller

In this section, the proposed string stable controller is designed and its characteristics are analyzed.

We are more interested in the performance of the platoon than that of the individual vehicle. Hence, we use the simple linear vehicle model, including two poles at the origin.

Figure 6.1 shows the notations and concept of the platoon with a finite number of vehicles following the leader vehicle. x_0 denotes the position of the leader vehicle while x_1 and x_i denote the position of the first and the i^{th} following vehicle. δ denotes the desired distance between vehicles. The leader vehicle will follow the reference positions, x_r , in an emergency braking situation, then the Laplace transform of its position is represented as,

$$X_0(s) = H(s)U_0(s) \tag{6.2}$$

where $H(s)$ and $X_0(s)$ denotes the transfer function of the vehicle model and position.

The control input of the leader vehicle, $U_0(s)$ is determined by,

$$U_0(s) = K(s)E_0(s), \tag{6.3}$$

where $E_0(s)$ represents the error defined by

$$E_0(s) = X_r(s) - X_0(s), \tag{6.4}$$

and $K(s)$ represents the linear transfer function of the controller for the leader vehicle. By plugging the equation 6.2 into 6.4, and 6.4 into 6.3, we get the transfer function from reference trajectory to the control input as follows.

$$U_0 = \frac{K(s)}{1 + H(s)K(s)} X_r(s) \tag{6.5}$$

Next, the position of the i^{th} vehicle can be expressed as follows.

$$X_i(s) = H(s)U_i(s) + \frac{x_i(0)}{s} \quad (i = 1, 2, ...n), \tag{6.6}$$

where $x_i(0)$ denotes the initial position of the i^{th} vehicle and denotes the control input to the i^{th} vehicle. The initial position of each i^{th} following vehicle is assumed to be $-i\delta$.

Then, the control input is decided by the following equation,

$$U_i(s) = K_p(s)E_i(s) + K_r(s)\Big(X_r(s) - X_i(s) - \frac{i\delta}{s}\Big) \quad (i = 1, 2, ...n), \tag{6.7}$$

where $X_r(s)$ denotes the desired reference trajectory position for the platoon. $E_i(s)$ denotes the error between the $i-1^{th}$ vehicle and the i^{th} vehicle defined as follows,

$$E_i(s) = X_{i-1}(s) - X_i(s) - \frac{\delta}{s}. \tag{6.8}$$

Notice that the control input 6.7 is expressed by the summation of two parts. In the first part, $K_p(s)$ represents the transfer function of the preceding vehicle following controller. In the second part, $K_r(s)$ represents the transfer function of the reference trajectory following controller. Because it is the summation of the two controllers, the following vehicles will maintain the desired distance, δ , while keeping the desired distance from the leader vehicle $i\delta$. We feed back the reference trajectory position instead of the leader vehicle position, because it is the desired trajectory that the platoon should follow in the case of an emergency braking situation.

Consider the closed loop error dynamics of this string stable controller. Combining equations 6.2, 6.3 and 6.4, we get equation 6.9.

$$E_0(s) = \frac{1}{1 + H(s)K(s)} X_r(s) \tag{6.9}$$

Similarly, by combining 6.6, 6.7 and 6.8, we get the following error relations.

$$E_1(s) = \frac{H(s)\{K(s) - K_r(s)\}}{1 + H(s)\{K_p(s) + K_r(s)\}} E_0(s) \equiv T_1(s)E_0(s) \tag{6.10}$$

$$E_i(s) = \frac{H(s)K_p(s)}{1 + H(s)\{K_p(s) + K_r(s)\}} E_{i-1}(s) \equiv T(s)E_{i-1}(s) \tag{6.11}$$

From above relations, it is clear that if $|T(j\omega)$ is larger than 1 at some frequencies, then error will amplify rearward and the platoon will become "string unstable". However, the feedback of the reference position provides us with the freedom to make below 1 at all frequencies. If we do not have the reference position feedback term, then $K_r(s) = 0$ and $T(s)$ becomes,

$$T_0(s) = \frac{H(s)K_p(s)}{1 + H(s)K_p(s)} \tag{6.12}$$

where $H(s)$ has two poles at $s = 0$. By the pole at the origin, bode magnitude plot of $T_0(s)$ will start from $T_0(0) = 0$ and may increase above 1. Even if it does not increase above 1, we still we get $\|T_0(s)\|_\infty = 1$ and if it does, we get $\|T_0(s)\|_\infty \geq 1$. It is clear that with input having a frequency component ω where $T_0(j\omega) \geq 1$, error will increase rearward in the platoon. One example of $T_0(s)$ and $T(s)$ is given in figure 6.2 using the system and controller parameters of the example given in the section 6.5. The figure shows that $T_0(s)$ has its peak value of 1.37, while $T(s)$ has peak value of 0.62.

In this section, the string stable controller for the platoon is designed and the attenuation of the error has been discussed. In the next section, how the designed controller outputs the control input along the platoon is discussed.

6.4 Peak Deceleration Amplification

As explained in section 6.2, we want to design a control strategy that does not command input exceeding the actuator limits. In this section, the relations between the reference position trajectory and the following vehicle's control input will be discussed. This relation will give us a way of regulating the following vehicle's control input below its limit by regulating the reference position trajectory. By manipulating equation 6.7 as follows, it is shown

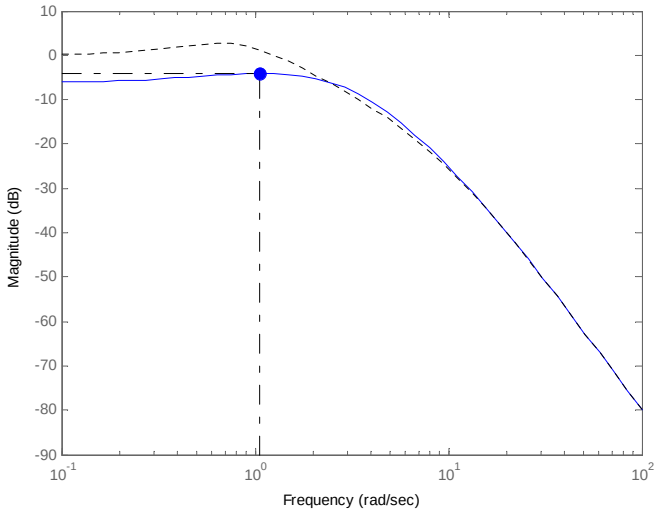

Figure 6.2: Transfer function of $T(s)$ and $T_0(s)$ given $H(s)$ and $K_p(s)$ as in equation 6.18 and 6.20. $\|T(s)\|_\infty = 0.62$ and $\|T_0(s)\|_\infty = 1.37$

that the control input of the i^{th} vehicle can be expressed by the summation of errors.

$$\begin{aligned} U_i(s) &= K_p(s) E_i(s) + K_r(s) \Big\{ X_r(s) - X_0(s) + X_0(s) \\ &\quad -X_1(s) + X_1(s) - ... + X_{i-1}(s) - X_i(s) - \frac{i\delta}{s} \Big\} \\ &= K_p(s) E_i(s) + K_r(s) \sum_{j=0}^{i} E_j(s) \end{aligned} \tag{6.13}$$

Using equations 6.9 and 6.10 6.11, we can make equation 6.13 represented by the reference input as follows.

$$
\begin{aligned}
U_i(s) &= \left\{ K_p(s)\, T_1(s)\, T^{i-1}(s) + K_r(s) \left\{ 1 + T_1(s) \sum_{j=0}^{i-1} T(s)^j \right\} \right\} \\
&\quad \times \frac{X_r(s)}{1 + H(s)\, K(s)} \\
&= \left\{ K_p(s)\, T_1(s)\, T^{i-1}(s) + K_r(s) \left\{ 1 + T_1(s) \sum_{j=0}^{i-1} T(s)^j \right\} \right\} \\
&\quad \times \frac{U_r(s)}{s^2 \{1 + H(s)\, K(s)\}} \\
&\equiv F_i(s) U_r(s) \qquad (i = 1, 2, \cdots, n),
\end{aligned} \tag{6.14}
$$

where $U_r(s)$ represents the acceleration of reference trajectory equivalent to $s^2 X(s)$. The above equation allows us to define the relationship between $U_i(s)$ and $U_{i-1}(s)$ as follows,

$$
\begin{aligned}
\frac{U_i(s)}{U_{i-1}(s)} &= \frac{K_p(s)\, T_1(s)\, T^{i-1}(s) + K_r(s) \left\{ 1 + T_1(s) \sum_{j=0}^{i-1} T^j(s) \right\}}{K_p(s)\, T_1(s)\, T^{i-2}(s) + K_r(s) \left\{ 1 + T_1(s) \sum_{j=0}^{i-2} T^j(s) \right\}} \\
&= \frac{K_p(s)\, T_1(s)\, T^{i-1}(s) + K_r(s) \left\{ 1 + T_1(s) \sum_{j=0}^{i-1} T^j(s) \right\}}{K_p(s)\, T_1(s)\, T^{i-1}(s)\, L(s) + K_r(s) \left\{ 1 + T_1(s) \sum_{j=0}^{i-1} T^j(s) \right\}}
\end{aligned} \tag{6.15}
$$

where $L(s)$ is

$$
L(s) = \frac{1 + H(s)\, K_p(s)}{H(s)\, K_p(s)}. \tag{6.16}
$$

Comparing the numerator and denominator of equation 6.15, it can be noticed that the difference is the multiplicative term $L(s)$. In the previous section, it is shown that the inverse of this term is $T_0(s)$ shown in 6.12, and this term is larger or equal to 1 at some frequencies. Thus equation 6.15

can be larger than or equal to 1, which means that more control input will be commanded to vehicles in the rear of the platoon. However, notice that equation 6.14 shows that the increase of the control input is due to the summation of the geometric sequence and the ratio of the sequence is smaller than 1. Therefore, the summation of the sequence will converge to a finite value while i goes to infinity.

Let $u_i(t)$, $u_r(t)$ and $f_i(t)$ be the impulse response of $U_i(s)$, $U_r(s)$ and $F_i(s)$. Then, in the time domain, equation 6.14 can be converted into the following inequality [15].

$$\|u_i(t)\|_\infty \leq \|f_i(t)\|_1 \|u_r(t)\|_\infty \tag{6.17}$$

where $\|u_j(t)\|_\infty$ denotes the $\sup_{t\geq 0} |u_j(t)|$ and $\|f(t)\|_1$ denotes $\int_0^\infty |f(t)|\,dt$.

From the above inequality 6.17, it is shown that the possible control input of the i^{th} vehicle, $\|u_i(t)\|_\infty$, can be calculated given $\|f(t)\|_1$ and the maximum acceleration of the reference position trajectory, $\|u_r(t)\|_\infty$. In the next section we will consider a numerical example and find the approximate limit for $\|u_i(t)\|_\infty$.

6.5 Numerical Example

In this section, we will show an illustrative example and analyze the behavior of control input and the following system response.

Let all the vehicles in a platoon be modeled with the same transfer functions as follows,

$$H(s) = \frac{1}{s^2(0.1s+1)} \tag{6.18}$$

The leader and the following vehicle controllers are designed with the transfer functions shown in equation 6.19 and 6.20.

$$K(s) = \frac{2s+1}{0.1s+1} \tag{6.19}$$

$$K_r(s) = K_p(s) = \frac{s+0.5}{0.1s+1} \tag{6.20}$$

The trajectory of the reference position, $x_r(t)$, is generated by integrating the acceleration shown in figure **??** twice. The generated reference velocity is plotted in figure **??** assuming that the initial velocity is 10 m/s.

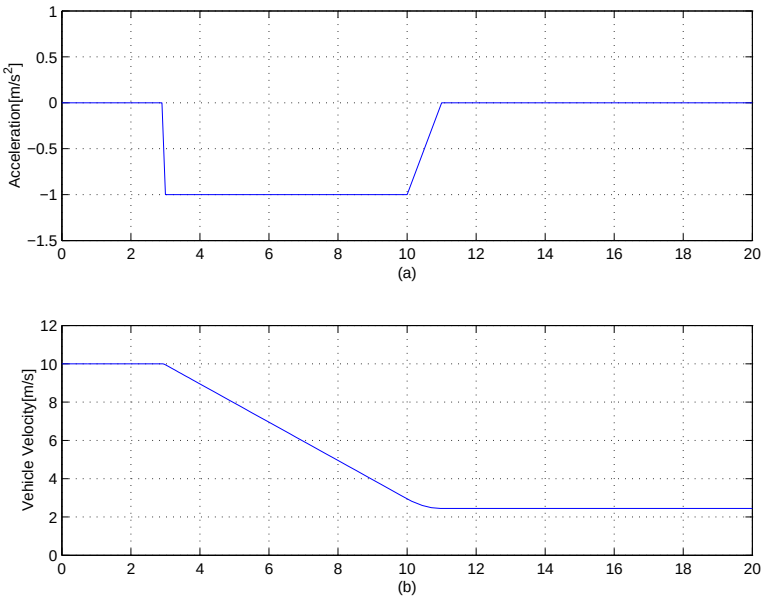

Figure 6.3: (a) Reference trajectory acceleration. (b) Reference trajectory velocity with initial velocity 10 m/s.

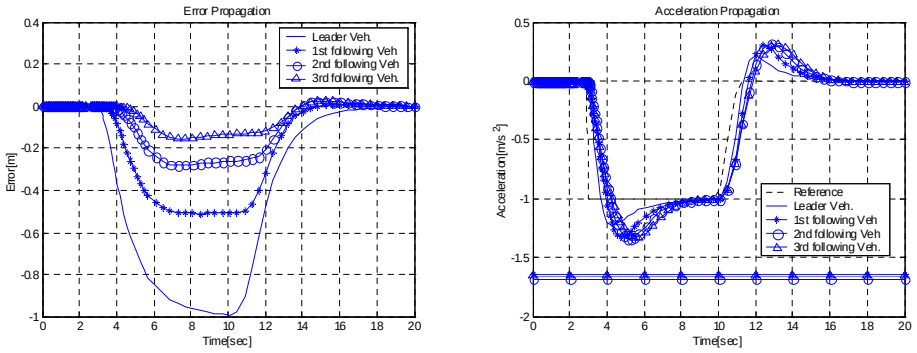

(a) (b)

Figure 6.4: (a) Error of the following vehicle with $K_p(s) = K_r(s)$. (b) Acceleration of the following vehicle $K_p(s) = K_r(s)$.

The simulation results of the designed controller are plotted in figure 6.4 (a) and 6.4 (b). It is shown that the errors attenuate for vehicles towards the rear of the platoon. This is because $T(j\omega) \leq 1$ for all ω, as shown in the figure 6.2.

In figure 6.4 (b), it is shown that the absolute values of the peak accelerations are increasing. However, this increment is very small due to the factor $T^{i-1}(s)$ multiplied by $L(s)$ in equation 6.15. Also in figure 6.4 (b), the bounds for the possible control inputs, $\|f_i(t)\|_1 \|u_r(t)\|_\infty$, are plotted below the acceleration curves. From figure 6.3 (a), we know $\|u_r(t)\|_\infty$ equals to 1, and the term $\|f_i(t)\|_1$ is calculated by integrating the absolute value of the impulse responses of $F_i(s)$ numerically. In this result, it is shown that for a unit step-like reference acceleration shown in figure 6.3 (a), the controllers of the following vehicles command desired acceleration around -1.6 -1.7 m/s^2 to the actuators. If this value is within the saturation limit of the actuator, the vehicles will show good performances. Otherwise, we have commanded too much deceleration on the reference trajectory, and may regulate the reference trajectory more.

It is shown in the previous section that the control inputs are eventually bounded no matter how large platoon we have, but it is difficult to get this bound because it is the sum of the sequence of transfer functions. However, the finite sum of the series will be enough to approximate the bounds because it increases slower for higher i^{th} term. In another simulation, $K_r(s)$ is

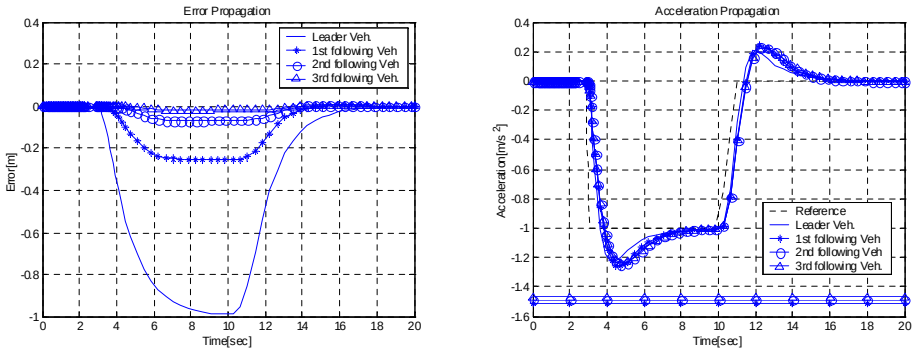

(a) (b)

Figure 6.5: (a) Error of the following vehicle with $3K_p(s) = K_r(s)$. (b) Acceleration of the following vehicle $3K_p(s) = K_r(s)$.

multiplied by 1.5 and $K_p(s)$ is multiplied by 0.5 in order to make the controller affected more by the reference position than by the preceding vehicle position. In figure 6.5 (a), the errors of the each vehicle are shown, and they show almost similar results with previous ones attenuating errors rearward. As the following vehicles are braking faster than before, the absolute values of the peaks are less than before. Therefore, it is shown in figure 6.5 (b) that the absolute values of the bounds have become smaller than the previous results. It is a desirable characteristic for the emergency braking controller to have less overshoot in its control input. However, giving too much portion to controller gain of the reference position side can give undesirable effects, i.e. the platoon will become less sensitive to the disturbance of the previous vehicle. Therefore, reasonable compromise should be made in determining the portion of the controller gain for the preceding vehicle following and reference trajectory following.

Chapter 7

Conclusion

1. We built mathematical models of vehicles under adaptive cruise control and cooperative adaptive cruise control. We implemented the models in two simulations to comparatively study the performance of the two control schemes on both microscopic and macroscopic level. The detail of the work is summarized in Chapter 2. A few conclusions drawn from the simulation results are listed below.

    - Vehicle-vehicle/Roadside-vehicle communication brings benefit to the highway traffic in increasing average velocity, decreasing braking effort, smoothing shock wave, and shortening the queue length of merging vehicles. Given all other conditions same, A CACC system almost always outperforms an autonomous ACC system in efficiency with less cost.
    - Higher market penetration is beneficial for both ACC and CACC systems in terms of average vehicle velocity, braking effort, and merging queue length.
    - With other conditions same, an aggressive controller design increases the average velocity, therefore enhances the efficiency. However a weaker controller saves braking effort.
    - V-V communication designed on basis of location based broadcast and event-driven has no appreciable influence for controlling vehicles in braking scenario in OVC.

    The many encouraging results justify the motivation of implementing V-V/R-V communication into vehicles control applications. The im-

portant work now is to design protocols as well as hardware to realize such communication with high Quality of Service (i.e. low probability of failure, short time delay) and low cost (i.e. low channel occupancy, low cost or no need for infrastructure construction, low increase in the vehicle price, etc.). This task is partially accomplished in the work summarized in Chapter 3.

2. In Chapter 3, the concept of location based broadcast is introduced for vehicle-vehicle communication in 5.9 GHz DSRC spectrum. The communication requirements of highway safety applications are discussed. A LBB protocol is designed and mathematically analyzed. The performance of the protocol is evaluated under wide range of communication parameters and highway traffic conditions.

   The future improvements of the LBB protocol include addition of selective acknowledgments, carrier sensing, situation-based adaptive transmission power control, and exploration on other coding schemes than repetition code.

3. In Chapter 4, the primary task of this research is to accurately obtain the slip of a wheel. First, a fifth wheel is used to obtain the accurate velocity of the vehicle, and the angular velocity of each wheel is measured. To obtain the circumferential velocity, the exact tire radius is needed. The change in the spring constant based on tire air pressure is obtained, and also the increase in tire radius due to the faster velocity is considered. The normal force applied on each wheel due to the pitch motion resulting from acceleration and deceleration is estimated. Brake torque sensor and accelerometer are used to find the normal force. Using the estimated normal force and road force, the tire-road friction coefficient is obtained. Also, the slip-friction coefficient curves under two different road conditions, dry and wet, are examined. First, on two types of roads the brake pressure is linearly increased to obtain full slip curve, and the maximum friction coefficient is estimated. Also, under two types of road conditions, the different slopes of slip-friction coefficient are definitely distinguished from each other, having slip in the range -0.02–0.02. In actual driving situations, current road condition needs to be judged, and therefore, recursive least squares is used to obtain slip slope in real time. However, in order to obtain the maximum friction coefficient with the observed slip slope, an algorithm based on

the brush model of a tire is needed. This research gives a foundation on emergency braking control by providing a method of maximum friction coefficient estimation.

4. In Chapter 5, a new vehicle longitudinal motion controller is suggested. The availability and the the performance of the controller is checked through simulation and compared with the previously used control method. A new method shows a better performance with smaller space tracking error than limited slip assumption controller in the simulation. However, the difficulty lies in measuring the precise slip data and heavy data handling for the implementation of the method. Also, the the fast slip dynamics are hard to catch using the current actuator with inevitable time delay. As a result, the new control strategy is not recommended with the existing level of technology.

   Emergency braking maneuvers of the vehicle following the current control scheme of the longitudinal motion has been analyzed with experimental vehicle. Within the bounds of deceleration limits that the vehicle can follow the controller with the limited slip assumption showed good performance.

5. In Chapter 6, a methodology for using a string stable controller in an emergency braking situation is presented. To avoid brake saturation and the subsequent wheel skidding one should reasonably bound the leader vehicle's allowable deceleration. To regulate the peak deceleration of the control inputs, we used the one norm of the impulse response function, which is acquired from the transfer function of reference trajectory deceleration to the i^{th} vehicle controller input. By dividing the deceleration limits of each following vehicle with this one norm of the impulse response, and then taking the minimum quotient over the string of vehicles, we can get the maximum allowable deceleration for the reference trajectory. Subsequently, the actuator saturation will not occur and the rear end collisions in the platoon can be avoided. In the beginning of this paper, we made several assumptions regarding the availability of communication and knowledge of friction coefficients between the road and tire, which are not yet practical in most vehicles. However, this study shows how the development of the communication and sensor technology can increase the safety in an advanced transportation system.

Bibliography

[1] http://www.leearmstrong.com/dsrc/dsrchomeset.htm.

[2] http://www.path.berkeley.edu/shift/.

[3] http://pems.eecs.berkeley.edu.

[4] http://path.berkeley.edu/DSRC.

[5] National automated highway system consortium c3 interim report. Technical Report Phase 1, October 1996-March 1998.

[6] K. Ahmed. *Modeling Driver's Acceleration and Lane Change Behavior*. PhD thesis, MIT, 1999.

[7] L. Alvarez and R. Horowitz. Hybrid controller design for safe maneuvering in the path ahs architecture. *Proceedings of the American Control Conference*, 1997.

[8] A. Bose and P. Ioannou. Analysis of traffic flow with mixed manual and semi-automated vehicles. Technical Report UCS-ITS-PRR-99-14, California PATH, 1999.

[9] Eichhorn U. Breuer, B. and J. Roth. Measurement of tyre/road friction ahead of the car and inside the tyre. *Proceedings of AVEC 92 (International Symposium on Advanced Vehicle Control)*, 1992.

[10] L. Briesemeister and G. Hommel. Disseminating messages among highly mobile hosts based n inter-vehicle communication. *IEEE Intelligent Vehicle Symposium*, 2000.

[11] T. Chang and I. Lai. Analysis of characteristics of mixed traffic flow of autopilot vehicles and manual vehicles. *Transportation Research Part C: Emerging Technologies*, 5C(6):333–348, December 1997.

[12] TRB National Research Council. *Highway Capacity Manual Special report 209*. 1985.

[13] M. Cremer, C. Demir, S. Donikian, S. Espie, and M. McDonald. Investigating the impact of aicc concepts on the traffic flow quality. *Fifth World Congress on Intelligent Transportation Systems*, 1998.

[14] S. Darbha and K.R. Rajagopal. Intelligent cruise control systems and traffic flow stability. *Transportation Research Part C: Emerging Technologies*, 7C(6):329–352, December 1999.

[15] C. A. Desoer and M. Vidyasagar. *Feedback Systems:Input-output Properties*. Academic Press, 1975.

[16] N. Every. Sae tirebraking tractin survey: A comparison of public highways and test surfaces. *Transactions of the SAE*, SAE 890638:735–742, 1989.

[17] A. Fritz and W. Schielen. Nonlinear acc in simulation and measurement. *Vehicle System Dynamics*, 36(2-3):159–178, September 2001.

[18] T. D. Gillespie. *Fundamental of Vehicle Dynamics*. Society of Automotive Engineers, Warrendale. PA, 1976.

[19] J. Glimm and R. E. Fenton. An accident-secerity analysis for a uniform spacing headway policy. *IEEE Transactions of Vehicular Technology*, VT-29(1), 1988.

[20] D. Godbole, N. Kourjanskaia, R. Sengupta, and M. Zandonadi. Breaking the highway capacity barrier: Adaptive cruise control-based concept. *Transportation Research Record*, (1679):148–157, 1999.

[21] D. Godbole and J. Lygeros. Safety and throughput analysis of automated highway systems. Technical Report UCB-ITS-PRR-2000-1, California PATH, 2000.

[22] F. Hall, V. Hurdle, and H. James. Synthesis of recent work on the nature of speed-flow and flow-occupancy (or density) relationships on freeways. *Transportation Research Record*, 28(1365):12–18, 1992.

[23] J.K. Hedrick, D. Godbole, R. Rajamani, and P. Seiler. Stop and go cruise control final report. http://vehicle.me.berkeley.edu/Publications/AVC/pqixu_vtc02.ps.

[24] K. Hedrick, Q. Xu, and M. Uchanski. Enhanced ahs safety through the integration of vehicle control and communication. Technical Report UCS-ITS-PRR-2001-28, California PATH, 2001.

[25] E. Hoffman and R. Mortimer. Scaling of relative velocity between vehicles. *Accid. Anal. And Prev.*, 28(4):415–421, 1996.

[26] T. Iijima, A. Higashimata, S. Tange, and et. al. Development of an adaptive cruise control system with brake actuation. *Intelligent Vehicle Systems*, (SAE SP-1538):173–178, 2000.

[27] A. Kato, K. Sato, and M. Fujise. Wave propagation characteristics of inter-vehicle communication on an expressway. *Eigth World Congress on Intelligent Transportation Systems*, 2001.

[28] H. Krishnan. personal communication.

[29] D. Lee, A. Attias, A. Puri, R. Sengupta, S. Tripakis, and P. Varaiya. A wireless token ring protocol for intelligent transportation systems. *IEEE 4th International Conference on Intelligent Transportation Systems, Oakland, CA*, 2001.

[30] Alvarez L. Li, P. and R. Horowitz. Ahs safe contgrol law for platoon leaders. *IEEE Transactions of Control Systems Technology*, 5(6), 1997.

[31] J. Lygeros and N. Lynch. Conditions for safe deceleration of strings of vehicles. Technical Report UCB-ITS-PRR-2000-2, California PATH, 2000.

[32] M. Minderhoud and P. Bovy. Impact of intelligent cruise control in motorway capacity. *Transportation Research Record*, (1679):1–9, 1999.

[33] R. Morris, J. Jannotti, K. Kaashoek, J. Li, and D. De Couto. Carnet: A scalable ad hoc wireless network system. *9th ACM SIGOPS European workshop, Kolding, Denmark*, 2000.

[34] Uchanski M. Müller, S. and J. K. Hedrick. Slip-based tire-road friction estimation during braking. *Proceedings of IMECE (ASME International Engineering Congress and Exposition)*, 2001.

[35] Department of Transportation of California. California highway design manual. *Transportation Research Record*, 1995.

[36] B.S.Y. Rao and P. Varaiya. Flow benefits of autonomous intelligent cruise control in mixed manual and automated traffic. *Transportation Research Record*, (1408):36–43, 1993.

[37] Pant A. Seiler, P. and J. K. Hedrick. Disturbance propagation in large interconnected systems. *Proceedings of the American Control Conference*, 2002.

[38] A. Shrivastava and P. Li. Traffic flow stability induced by constant time headway policy for adaptive cruise control vehicles. *American Control Conference, Chicago, Illinois*, June 2000.

[39] J. Singh, N. Bambos, B. Srinivasan, and D. Clawin. Wireless lan performances under varied stress conditions in vehicular traffic scenarios. *IEEE Vehicular Technology Conference, Vancouver, Canada*, 2001.

[40] B. Song and D. Delorme. Human driver model for smartahs based on cognitive and control approach. *Proceedings of the 10th Annual Meeting of the Intelligent Transportation Society of America*, 2000.

[41] D. Swaroop and Hedrick J. K. String stability of interconnectied sytems. *IEEE Transactions on Automated Control*, 41(4):349–356, 1996.

[42] B. van Arem, J. Hogema, M. Vanderschuren, and C. Verheul. An assessment of the impact of autonomous intelligent cruise control. *TNO Report INRO-VVG, Netherlands*, March 1996.

[43] J. VanderWerf, N. Kourjanskaia, S. Shladover, H. Krishnan, and M. Miller. Modeling the effects of driver control assistance systems on traffic. *U.S. National Research Council Transportation Research Board 80th Annual Meeting*, January 2001.

[44] Q. Xu, K. Hedrick, R. Sengupta, and J. VanderWerf. Effects of vehicle-vehicle/roadside-vehicle communication on adaptive cruise controlled highway systems. *IEEE Vehicular Technology Conference*, October 2002.

[45] Q. Xu, D. Jiang, and R. Sengupta. Design and analysis of highway safety communication protocol in 5.9 ghz dedicated short range communication spectrum. *IEEE Vehicular Technology Conference*, April 2003.

[46] Y. Yamamura, M. Tabe, M. Kanehira, and T. Murakami. Development of an adaptive cruise control system with stop-and-go capability. *Intelligent Vehicle Initiative: Technology and Navigation Systems*, (SAE SP-1593):37–44, 2001.

[47] T. Yokota, M. Kuwahara, and H. Ozaki. A study of ahs effects on traffic flow at bottlenecks. *Fifth World Congress on Intelligent Transport Systems*, October 1998.

[48] T. Yokota, S. Ueda, and S. Murata. Evaluation of ahs effect on mean speed by static method. *Fifth World Congress on Intelligent Transport Systems*, October 1998.

[49] M. Zennaro and J. Misener. A state-map architecture for safe intelligent intersection. *ITSA, Minneapolis*, 2003.

[50] P. Zwaneveld and B. van Arem. Traffic efffects of automated vehicle guidance systems. *Fifth World Congress on Intelligent Transportation Systems*, October 1998.